Titre: Title:	Closed-loop Automation of Shot Peen Forming with In-process Shape Measurements
Auteur: Author:	Wassime Siguerdidjane
Date:	2022
Type:	Mémoire ou thèse / Dissertation or Thesis
Référence: Citation:	Siguerdidjane, W. (2022). Closed-loop Automation of Shot Peen Forming with In-process Shape Measurements [Ph.D. thesis, Polytechnique Montréal]. PolyPublie. https://publications.polymtl.ca/10171/

POLYTECHNIQUE MONTRÉAL

affiliée à l'Université de Montréal

Closed-loop automation of shot peen forming with in-process shape measurements

WASSIME SIGUERDIDJANE

Département de génie mécanique

Thèse présentée en vue de l'obtention du diplôme de *Philosophiæ Doctor*

Génie mécanique

Janvier 2022

POLYTECHNIQUE MONTRÉAL

affiliée à l'Université de Montréal

Cette thèse intitulée :

Closed-loop automation of shot peen forming with in-process shape measurements

présentée par **Wassime SIGUERDIDJANE**

en vue de l'obtention du diplôme de *Philosophiæ Doctor*

a été dûment acceptée par le jury d'examen constitué de :

René MAYER, président

Farbod KHAMENEIFAR, membre et directeur de recherche

Frédérick GOSSELIN, membre et codirecteur de recherche

Sébastien LE DIGABEL, membre

Tsz Ho KWOK, membre externe

ACKNOWLEDGEMENTS

I would like to first thank my advisors Professors Farbod Khameneifar and Frédérick Gosselin. Frédérick introduced me to academic research during my undergraduate studies and offered me the master's project that became this PhD thesis. I first came to him for advice on finite element modelling and ended up learning more than I hoped on the topic and more during my graduate studies. Farbod, from his background in metrology, was an agent of precision and a constant reminder of its importance in my work, both in terms of measurement and writing.

I am grateful to Pr. René Mayer, Pr. Sébastien Le Digabel and Pr. Tsz Ho Kwok for accepting to be part of my thesis committee.

This work was possible due to the financial support and technical expertise provided by Aerosphère. I especially would like to thank Mr. Georges Hébert and Mr. Guy Levasseur for their key insights on the way shot peen forming is conducted in an industrial setting.

I would like to thank Dr. Hong-Yan Miao for her insights on shot peen forming and her comments on manuscripts. I would also like to thank all friends and colleagues at Polytechnique with whom I share fond memories. I am in particular grateful to Alexandre, Moustapha, the Oliviers, Pierre, Simon and Vlad.

Finally, I would like to thank Sonia for her daily support and encouragement, and my family for everything they do for me.

RÉSUMÉ

La mise en forme par grenaillage (shot peen forming) est comunément utilisée dans l'industrie de la fabrication aérospatiale pour mettre en forme des panneaux minces et corriger la distorsion dans des pièces usinées. Les impacts de projectiles introduisent des déformations plastiques et des contraintes résiduelles compressives en surface du matériau. Le procédé de mise en forme par grenaillage utilise ces déformations plastiques pour courber la pièce traitée. Ce phénomène s'explique par une incompatibilité géométrique entre la couche traitée qui s'étire suite à sa déformation plastique, et le reste du matériau qui force la flexion de la pièce. L'opérateur contrôle le processus en choisissant le type de projectiles utilisé, la vitesse des impacts, les régions de la surface de la pièce qui sont traitées et le temps de bombardement. Bien que le procédé de mise en forme par grenaillage ait été utilisé depuis les années 1950, il demeure manuel et basé sur l'intuition humaine d'experts, alors que les besoins industriels demandent une meilleure reproductibilité et précision. Pour cette raison, l'industrie se tourne vers l'automatisation. Des outils de simulation et par la suite de planification du procédé ont été développés pour mieux comprendre le procédé et atteindre son automatisation. Planifier le procédé est en soit un problème complexe car il demande d'anticiper comment la pièce se déforme, ce qui est généralement résolu par la méthode des éléments finis. Malgré la disponibilité d'outils numériques, la planification et la simulation de la mise en forme par grenaillage comportent toujours des erreurs importantes par rapport aux résultats expérimentaux. Ces erreurs sont principalement causées par la présence de contraintes résiduelles initiales dans le matériau. Les contraintes résiduelles initiales proviennent de l'historique de fabrication de la pièce et interfèrent avec les contriantes induites par le grenaillage, introduisant des erreurs de mise en forme. Des variations dans les procédés de fabication ultérieurs peuvent introduire des contraintes différentes d'une pièce à l'autre, puisque chaque étape de fabrication laisse ses propres contraintes résiduelles. Puisque les méthodes de mesure de contraintes résiduelles sont soit trop dispendieuses ou destructives, leur meusure durant le processus est non-trivial.

Pour dépasser cette limite, cette thèse explore la solution d'automatiser la mise en forme par grenaillage en boucle fermée, à l'aide de mesures de forme et de planification itérative, dans le but de réduire les erreurs et de compenser pour l'effet des contraintes résiduelles intiales. Cette thèse présente trois contributions principales sous la forme d'un réseau de neurones permettant de planifier la mise en forme par grenaillage en temps réel, une procédure de mise en forme en boucle fermée permettant de réduire l'erreur initiale de mise en forme, ainsi que le détail de la conception d'un robot de grenaillage à petite échelle permettant de réaliser des essais de validation expérimentaux à faible coût.

ABSTRACT

The aerospace manufacturing industry relies on shot peen forming to shape thin sheet metal components such as wing skin panels and correct distortions in machined structural components such as ribs. The process uses high-velocity projectile impacts to plastically deform a thin portion of the component and introduce compressive residual stress at the surface. In the case of shot peen forming, the plastic deformations that accompany the compressive stresses are leveraged to bend the part. The induced plastic deformations can be seen as the expansion of a layer at the surface of the material which is constrained by the unaffected layer that represents the rest of the material. This constraint introduces a geometric incompatibility that forces the part to bend. The process is controlled by choosing the size and the material of the projectiles, the velocity at which they impact the surface of the part, the exposure time of the part to the impacts and the location of treatment. Although it has been used in aerospace applications since the 1950s, the process remains manual in majority and is still anchored on expert knowledge and human intuition. Contrastingly, industrial needs are oriented towards better process accuracy and precision. A proposed solution to meet these needs has been the automation of the process. To increase the understanding of the process and build towards automation, numerical tools for simulating and planning the process have been developed. The planning of shot peen forming is inherently complex because determining each treatment action requires solving a solid mechanics problem to consider the effect of the process on the material. This is typically done through finite element simulations. Even when the mechanical problem is solved, discrepancies are observed between simulations and experiments. The main source of error in shot peen forming is explained by the presence of initial residual stresses in the material. Initial residual stresses are remnants of the part's manufacturing history. In the case of aluminum plates, the main source of initial residual stresses is the lamination process that the panels undergo during their production, but if a particular sample has been deformed in a press or machined in an ulterior production step,

different residual stresses have been introduced in the sample. For this reason, the initial stress state of parts may vary from sample to sample. The currently available methods to measure residual stresses being either prohibitively expensive or destructive, the in-process measurement of stresses is impractical. To address this limitation, this thesis explores the solution of using a closed-loop method based on in-process shape measurement and iterative re-planning to compensate for measured error and form more accurate aluminum plates into given target shapes.

TABLE OF CONTENTS

LIST OF TABLES

LIST OF FIGURES

CHAPTER 1 INTRODUCTION

When thinking about industrial sheet metal forming, one generally pictures large tooling comprised of dies and matrices. These tools are generally massive, expensive and can only manufacture a single part. On the other hand, when we consider most of human history, goods from thin sheets of metal have been crafted without the limitation of such rigid forming tooling. This analogy makes us consider the lone blacksmith imposing their will on the material with hammer and anvil. This crafts-person learned through experience how to control the shape of the metal under the impact of the hammer, offering a flexible method able to yield compound surfaces, notably used in armours. In the 1940s the Lockheed Aircraft Corporation patented an industrial application of a cold working process (Tatton, 1986) based on the controlled repetition of impacts on a thin sheet, which relies on a similar principle to hammer and metal interaction as conventional blacksmithing. This process, called shot peen forming, harnesses the impact energy of small projectiles called shot, usually hard steel spheres less than 3 mm in diameter, which act as multiple small hammers. Shot peen forming offers the flexibility of forming complex geometries without the need for dies and matrices. Varying the size, the material, the velocity of shot, and which region of the part is peened provides control over the resulting shape of the part.

Since it became available, the aerospace manufacturing industry has relied on shot peen forming to form thin sheet metal components and correct distortion in machined parts. To this day the process remains founded on expert knowledge and intuition gained through trial and error. The experience accumulated by industry leaders is mostly a well-kept trade-secret, which constitutes a challenge in assessing the actual state of the art of the field. The peen forming scientific community made progress in the development of process planning methods (VanLuchene and Cramer, 1996; Faucheux et al., 2018; Luo et al., 2020), but only considered

the sample plates to be initially stress-free. These unknown initial stresses represent the main source of deviation with the target in peen-formed parts. Since stress measurement methods are either expensive or destructive (Schajer, 2013), the field requires the development of a method that can adapt to their effect without knowing their nature, which constitutes the main automation challenge. The development of such a method, which does not exist yet, has the potential to address the lack of efficiency and repeatability of current practices. The objective of this thesis is to propose a solution to this problem in the form of a closed-loop method based on iterative peen forming and in-process measurements.

This thesis is structured as follows. Chapter 2 presents a critical review of the literature. Chapter 3 details the objectives and rationale of the thesis. Chapter 4 presents a first article resulting from this work, which demonstrates that an artificial neural network can be trained on data generated through finite element simulations to plan shot peen forming in real-time. Chapter 5 presents a second article which details the design of a low-cost small scale shot peen forming robot that was harnessed to demonstrate the closed-loop shot peen forming method proposed in this thesis. Chapter 6 presents a third article that proposes a closed-loop method for iteratively planning, forming, measuring and replanning shot peen forming to reduce the initial forming error involved in conventional open-loop planning of shot peen forming. This article exhibits an experimental test case that validates the method. Chapter 7 discusses the limitations of the current contribution and ideas for further improvements to the field of shot peen forming automation. Chapter 8 concludes the manuscript.

CHAPTER 2 LITERATURE REVIEW

2.1 The current state of shot peen forming

The main practical elements of shot peen forming are the shot media, the propulsion method and the method used to control when and where to impact the material. To verify the conformity of the formed part, an inspection method is required. The type of media affects the treatment via its size, mass and hardness. The propulsion method affects the treatment by controlling the velocity of the shot and the quantity of shot impacting the material at any time. The impact position control method determines which portions of the workpiece are to be treated, which is referred to as the peening pattern.

Currently, the shot peen forming industry mainly uses steel media of various sizes depending on the application and the required peening intensity (Champaigne, 1993). The main propulsion system used is a shot peening nozzle (Champaigne, 1993), such as that illustrated in Figure 2.1. In this system, compressed air is injected into the straight section of a tube, creating a zone of low pressure by the venturi effect in a branching angled section. This angled section is connected to the shot reservoir and acts as shot intake driven by the suction created by the low pressure. The media is projected toward the material with the compressed airflow. Finally, the main control method used is human operation. Figure 2.2 shows a close-up of a typical shot peen forming machine with a human operator holding a shot peening nozzle which is connected to a portable shot peening tank and air source. The figure further provides insight into how the operator controls the shot stream. The nozzle provides the user with a trigger to turn on the shot stream while the operator's hand acts as a shutter to control where the shot needs to impact the part.

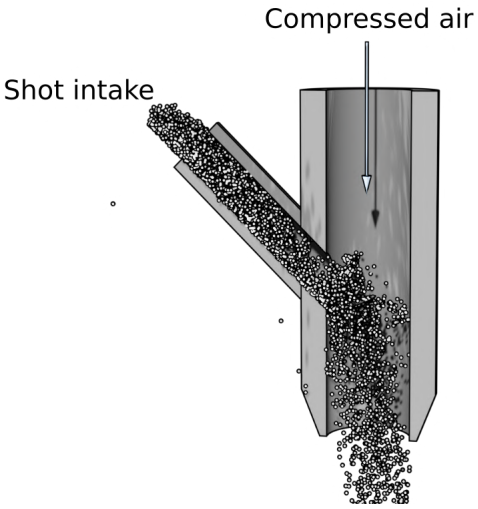

Figure 2.1 A rendered illustrating the principle of a venturi nozzle. The compressed air is injected in the straight intake on the nozzle, which creates low pressure in the side shot intake tube. This creates suction that projects the shot out of the nozzle.

To improve the repeatability, accuracy and efficiency, the aerospace industry turned towards the development of automated solutions. This gave rise to industrial solutions of nozzle-equipped shot peening robots enclosed in large blasting cabinets such as the installation presented in Figure 2.3.

Figure 2.2 An operator manually peen forming a part. The operator uses a gloved hand to block part of the nozzle during the treatment. The flow of shot is kept constant and the operator's hand acts as a control shutter. Reproduced with permission from Aerosphère Inc.

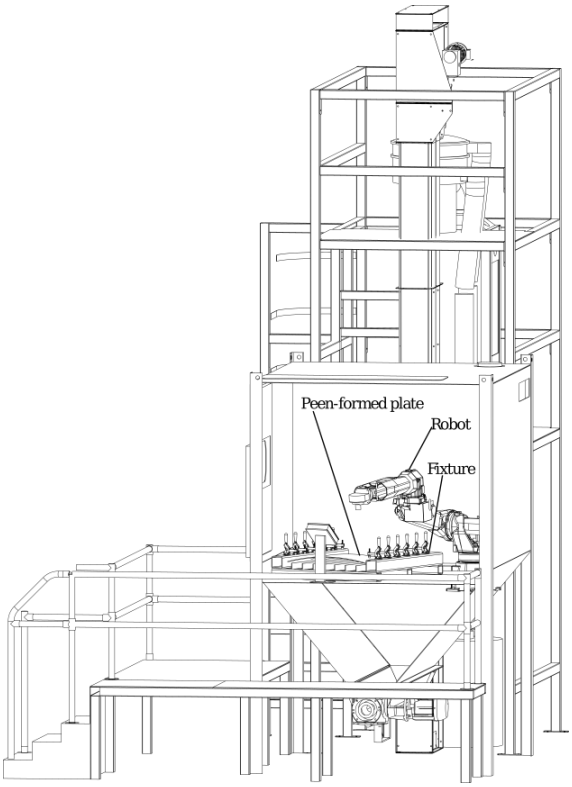

Figure 2.3 A model of a shot peening cabinet designed to house an industrial robot equipped with a shot peening venturi nozzle.

Currently, the industry validates the conformity of a formed part by checking its shape against a reference fixture (Ramati et al., 1999). In this inspection scenario, an inspector measures the gap between the part and the fixture with calibrated feeler gauges. Depending on the application, the part can be elastically deformed by placing a specified weight of sandbags on it (Ramati et al., 1999). In the context of airplane wing skins, this simulates the presence of rivets. The part is deemed suitable if the maximum gap between it and the reference is below a specified application tolerance. This method is robust in the context of human-operated forming but cannot realistically be automated. Automation demands accurate, repeatable and efficient measurement methods, such a 3D scanners or Coordinate Measuring Machines (CMM).

While numerically controlled machines and robotic arms can substitute a human operator

to deliver the shot to the part, automated shot peen forming presents further challenges. For instance, the accurate simulation and planning of the process, the measurement of peen-formed parts. The state of the art on these topics is reviewed next.

2.2 Mechanics of shot peen forming

Before simulation and planning methods can be introduced, it is necessary to consider the high-level phenomenon that governs the mechanical behavior of shot peen forming. This section presents a high-level view of the mechanics of shot peen forming.

Shot peen forming uses the impacts of the projected shot to plastically deform a thin layer of material near the treated surface. This plastic deformation can be represented as the expansion of the treated layer. Since the treatment only expands a shallow portion of the thickness, it creates a geometric incompatibility that bends the part (Ballard, 1991). This incompatibility of deformation results in compressive residual stresses near the treated surface, which are used in shot peening to reduce the propagation of surface cracks and increase the component's fatigue life (Gariépy et al., 2011). By controlling where the part is treated and how much that zone's affected layer expands, the process can form plates into complex geometries.

From the theory of thin shell mechanics, we understand that a plate's deformation can be expressed in terms of bending and stretching (Audoly and Pomeau, 2010). In shot peen forming, the stretching comes from the expansions of the treated portions of the material. If a plate is treated in the same zones on both sides, it will mostly deform in stretching. If only one side of the plate is treated in a given zone the main mode of deformation will be bending. In general, bending is the predominant deformation mode in shot peen forming (Chen et al., 2014). Figure 2.4 provides and illustration of the principle.

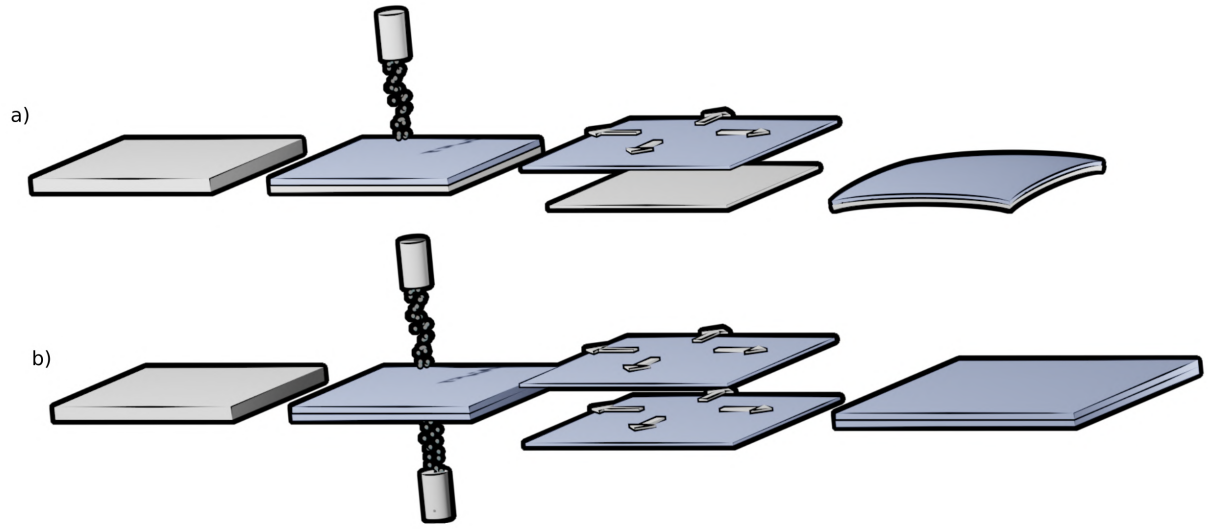

Figure 2.4 An illustration of the bending and stretching of peen formed plates explained with bilayer plates: (a) uniform single-sided peening stretches only one layer of the plate creates a geometric incompatibility that causes bending; (b) uniform double-sided peening of the plate causes stretching.

With non-linearity comes the potential for instability. As described in (Faucheux et al., 2018), for large displacements, shot peened plates exhibit an instability problem that manifests itself in the form of a curvature bifurcation. More practically, when uniformly treating one surface of a square plate, we expect to see an almost even deformation of the plate in both transverse directions, i.e. to deform in a spherical fashion. A small difference between the two in-plane directions of the plate is present due to the anisotropy introduced by the lamination process involved in the manufacturing of plates (Gariépy et al., 2013a). Although there is a difference in curvature in both directions, it is a small difference for small displacements. When large displacements are involved, this anisotropy pushes the instability mechanism to introduce a large discrepancy between the two directions. This makes the plate deform in a cylindrical fashion as opposed to spherical. Figure 2.5 provides an illustration of the principle. This

phenomenon is only present in perfectly square plates and causes problems only for niche applications requiring uniformly treated square plates, and most panels in aerospace are either rectangular or of more complex geometry. This spherical-to-cylindrical instability illustrates well the geometrical non-linear nature of thin plate mechanics. Therefore, care must be taken when simulating peen forming.

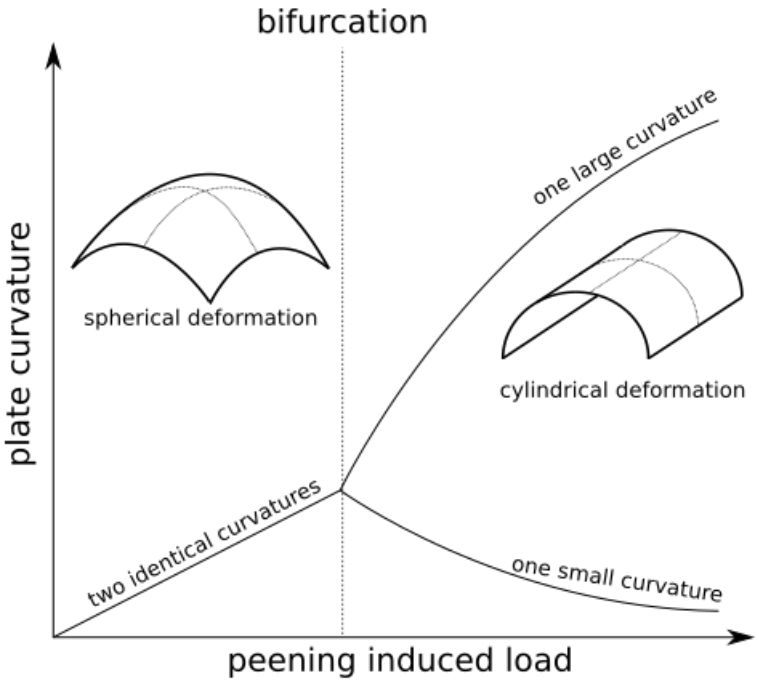

Figure 2.5 Illustrating the instability induced bifurcation of shot peened square plates: at low peening induced loads, a square plate exhibits two identical curvatures, hence a spherical deformation. At higher peening induced loads, the bifurcation phenomenon occurs. One curvature becomes considerably larger than the other, hence a cylindrical deformation.

2.3 Modelling of shot peen forming

Models simulate a predetermined course of actions and inquire about their potential results. The works focusing on this sub-field of shot peen forming either strive to replicate as accurately as possible the physical events involved in the process, or to replicate the indirect effects of the process on the material. Both modelling approaches are concerned with different levels of granularity. Some methods focus on understanding the local effects of impacts on the material, while others are concerned with the global effects of the process on the structure, and others combine both scale levels. Both approaches however desire to distill a model to represent as accurately as possible the mechanics of the process.

2.3.1 Local/global models

Local/global models are hybrid modelling approaches that combine an initial model that computes local features such as induced stresses with a global model that computes structure-wide features such as deflections. Impact-based modelling strategies generally harness this local/global approach by simulating every impact with specified process parameters to compute the induced residual stresses and plastic strains (Faucheux, 2019). The resulting deformed arc is obtained by a springback analysis. This step finds the rest configuration which results from the equilibrium of strains in the material. These methods are computationally expensive and provide local information such as induced stresses. Cao et al. (1995) leveraged the model proposed by Khabou et al. (1990) to compute the residual stresses induced by the shot peening treatment and used them as initial state in a springback analysis. Gariépy et al. (2011) and later Gariépy et al. (2013b) proposed a dynamic impact model that considers the effect of the progressive deformation of a shot peened coupon. Impact models such as the ones proposed by Miao et al. (2009); Gariépy et al. (2011); Gariépy et al. (2013b) harness finite element simulations, when semi-analytical models were previously used. Alternatively,

Chaise et al. (2012) proposed a hybrid solution that first computes the induced plastic strains using a semi-analytical impact model and introduces them in a finite element model as thermal strains. These thermal strains were implemented by assigning the average plastic strain value to the thermal expansion coefficient of the affected layer of the material. This method of implementing plastic strains as thermal strains provides a simple solution that can easily be implemented in commercial finite element software (Faucheux, 2019). This is commonly used to model bilayers that deform through incompatible strains in other scientific fields such as plant growth (Goriely, 2017), along with peen forming applications (Faucheux et al., 2018).

2.3.2 Global models

In contrast with the pure modelling endeavours, applied simulations require methods that can provide rapid approximations of the features of interest alone, while local/global models provide both stress fields and resulting nodal coordinates. In the case of applied peen forming, on the other hand, the only information required is the nodal coordinates of the deformed plate (Faucheux, 2019). For this reason, global models are more efficient at simulating the process in an applied context.

Global models simulate the effect of the global shape of the structure. They often rely on an approximation of average plastic strain induced by the peening treatment (Faucheux, 2019). Levers and Prior (1998) proposed to introduce the shot peening loads in a shell model using thermal strain approximated along discrete points in the thickness of the plate. This approximation of the plastic strains induced by the process can be seen as a series of discrete expanding layers of material. The plastic strains are further approximated as a single expanding layer in a bilayer model inspired by the active bilayers from the field of soft matter physics (Alben et al., 2011). Faucheux et al. (2018) further used this idea combined with the theory of eigenstrains, represented as thermal expansions. This modelling strategy re-

lies on the geometric incompatibility presented in Section 2.2 to compute the deformed rest configuration of the plate. Such models only provide geometric information in the form of resulting deformation, which is necessary for the evaluation of planned courses of actions in the automated process.

2.4 Planning of shot peen forming

Planning can refer to various parts of the shot peen forming process. It can imply the determination of the path a robot arm needs to take to perform a shot peening task. It can also imply the determination of the required task that must be accomplished. Robotic path planning being a field of research on its own, the current definition focuses on the planning of shot peen forming tasks. This section then focuses on the question of determining the required process parameters (effectiveness and pattern) for a plate to be formed into a given target shape.

The numerical representations provided by simulation tools offer an approximation of the behaviour expected from the material in reality. Such tools can be harnessed as part of planning algorithms, to determine the effect of potential candidate actions. While the literature presents a comprehensive selection of modelling strategies, only a limited set of numerical planning tools are available for the task of shot peen forming. This observation may be justified by the more applied nature of planning, as opposed to the more theoretical grounding of modelling, which is more tailored to the reality of academic research. Another pragmatic reason for such observation may lie in the competitive interests of applied technologies involved in planning an industrial process.

Among the planning methods presented in the literature, only a few focus on the planning of the complete set of process parameters required to peen form a part. Many examples such as (Delijaicov et al., 2010) focus only on planning the parameters related to the process intensity. In these works coupons or plates are uniformly treated and the goal of the planning is to determine, e.g. in the case of a nozzle-based system, the shot diameter, compressed air pressure and exposure time, to obtain a given deflection or curvature.

In contrast, a planning method that considers the full scope of parameters required to form a plate into an arbitrary target shape requires the addition of peening pattern planning. In other terms, knowing the intensity of the process is not sufficient to form complex shapes, the location in which the treatment is an additional factor to consider. The methods that consider the planning of peening patterns are of greater interest in the present study. These planning solutions stem from modelling solutions. The core concept of shot peen forming planning is to harness the model to test various plans proposed by the planning algorithm and determine which plan is likely to yield the deformation closest to the target shape. These optimization algorithms propose plans and chose the best based on a performance criterion in the form of loss function. Optimization algorithms can require the derivative of the defined loss function to find the solution which offers the lowest loss value. These gradient-based methods are known to generally converge faster since the gradient of the loss function provides a more detailed view of the objective function and the location of its optimums. The method proposed in (VanLuchene and Cramer, 1996) is grounded in the modelling strategy proposed in (Homer and Van Luchene, 1991). The method proposed in (Faucheux, 2019) and (Miao et al., 2021) harness the interior points optimization algorithm (Byrd et al., 1999) to find the optimal pattern in a simulation based on the model proposed in (Faucheux et al., 2018). The observation that simulation methods are used within planning methods reinforces the requirement for the chosen simulation method to be efficient since it will be called upon repeatedly during planning.

As mentioned in Section 2.2, the mechanics of shot peen forming are inherently non-linear, even if they can be approximated with linear models when small deformations are involved. For planning, on the other hand, even the approximation of linear mechanics in simulations requires solving a non-linear problem to obtain peen forming parameters such as the required peening pattern (Faucheux, 2019). As presented, the shot peen forming planning literature proposes the use of iterative optimization to solve this non-linear problem.

The advances in the field of machine learning, and Deep Learning, in particular, offer the opportunity of looking at this problem from a different angle. The performance of Artificial Neural Networks has been demonstrated on complex non-linear problems such as image classification (Krizhevsky et al., 2012), image segmentation (Shelhamer et al., 2017) and 3D data segmentation (Qi et al., 2017). Despite the popular belief that neural networks (NNs) are black boxes, they are actually non-linear function approximators, that fit complex non-linear functions from a given dataset (Goodfellow et al., 2016). From this definition, the usefulness of NNs in the context of shot peen forming planning is understandable due to the non-linear nature of the shot peen forming planning problem. While the shot peen forming literature presents a few contributions that leveraged a NN to predict peening intensity parameters to reach the desired curvature on a uniformly treated Almen strip (Delijaicov et al., 2010) or small coupon, none leverage NNs to compute peen forming patterns required to reach complex target shapes. This topic is further explored in Chapter 4. The main advantage of NNs when compared to iterative methods is that the NN training iterations can be handled off-line while other methods require in-process computations. This advantage makes the NN more suitable for real-time in-process planning. The main limitation of most NN solutions is the requirement to generate large datasets for the training (Goodfellow et al., 2016). Furthermore, this step of the process is likely to limit the quality of the learned function if the user accidentally introduces bias in the generated dataset (Tommasi et al., 2015). This

limitation introduces the notion of generalization. If a properly designed NN is trained using a well-balanced dataset that covers all the possible variations of a phenomenon, we could expect the NN to perform adequately on any possible input for the function that governs the physical phenomenon. Considering that the planning of a shot peen forming process for any given target shape involves a large number of possibilities which is exponentially proportional to the resolution of the simulation, it is impossible to test for all of them to prove the generalization of the NN. This leaves a profound question regarding the NN solution, which is yet to be answered.

2.5 The effect of initial residual stresses

The planning solutions proposed by the literature are all based on the hypothesis of ideal plates as defined by the numerical models they are grounded on. These idealized plates are assumed to be stress-free, isotropic, perfectly flat and homogeneous. These approximations introduce errors in the plan since the real plate cannot be considered ideal. The main factor contributing to these errors is the presence of initial residual stresses (Faucheux, 2019). These initial residual stresses are remnants of the material's previous manufacturing steps such as lamination in the case of plates (Prime and Hill, 2002). The effect of initial residual stresses on the formed shape is explained by the fact that shot peen forming uses stresses to control the shape of parts. If stresses are already present in the part, they will interfere with the induced forming stresses. This leads, if unaccounted for, to errors that are unpredicted by planning and simulation programs.

One approach for handling these imperfections would be to alter the model to take into account the initial shape and the initial residual stress field of the plate. For this, both the initial shape and the initial stress state of the plate would need to be measured. In the case of shape measurement, this solution is viable with the measurement methods pre-

sented in Section 2.6, but the measurement of residual stress profiles is a more delicate topic. Residual stresses can be measured through various methods that can be either destructive postmortem methods and non-destructive methods (Schajer, 2013). If one is interested in characterizing stresses on test samples a posteriori, destructive methods can be considered, but for final products this is impossible. Since the initial stress state of a plate is crucial to shot peen forming automation, it would be logical to consider using a non-destructive stress measurement method in the planning workflow to identify the initial stresses and take them into account when planning. The main reason for the lack of adoption of in-process stress measurement in shot peen forming seems to stem from the prohibitive cost of non-destructive stress measurement, which mostly relies on diffraction of rays (Schajer, 2013). These methods require tailored laboratory equipment not likely to be installed adjacent to destructive projectile scattering shot peening equipment. For these reasons, in-process residual stress measurements for shot peen forming have remained in the realm of the plausible but impractical given the current state of commonly available stress measurement technology. However, the future of automated shot peen forming may benefit from in-process stress measurement with the help of commercial ventures such as the X-Raybot from MRX (MRX, 2021), which strives to make stress measurement more accessible and automated.

Since we can describe the mechanics of shot peen forming in terms of the expansions of a bilayer plate, a given configuration is only the result of the equilibrium of bending moments about the plate's thickness. This bending moment equilibrium is the result of the bilayer expansions that result from the residual stress-induced plastic strains caused by the repeated impacts. With these conventions, the initial residual stresses can be considered indirectly in terms of the effect they have on the observed shape of the plate. This describes the basis for the paradigm of closed-loop planning presented in Chapter 6. It offers the possibility of executing the plan, observing the result and adjusting the plan to take into account the observed errors.

2.6 Measuring peen-formed plates

Every shape measurement method comes with its sources of uncertainty. The field of metrology has for objective to reduce and quantify the sources of uncertainty in these measurements. The required method depends on the application, and the scrutiny with which the part can be inspected depends on the uncertainty of the measurement method. Contact and non-contact methods form the principal classes of 3D coordinate measurement methods. Both classes of methods acquire sets of points on the part surface forming point clouds. Contact probes on a coordinate measuring machine (CMM) exhibit a data acquisition rate of tens of points per second (Li and Gu, 2004) with high accuracy of up to a few microns (Prieto et al., 2002), while non-contact methods offer less accurate measurements (tens of microns) (Ghandali et al., 2019; Bonin et al., 2021) at faster acquisition rates (thousands of points per second) (Li and Gu, 2004). The requirement for a tactile probe to touch the measured surface explains the low acquisition rate of contact methods.

Optical 3D scanning methods such as structured light and laser triangulation methods rely on the projection of a reference source of light. In the context of laser scanning, a laser beam's distortion is measured as an out-of-plane deformation of the measured surface (Lanman and Taubin, 2009). By knowing the camera's position and angle with respect to the laser diode, the coordinates of each point on the curve defined by the laser beam can be computed through triangulation. It is mathematically sound to view this process as the measurement of points on the intersection of a plane and an object of arbitrary shape. The laser is then swept along the object's surface to perform multiple measurements. In the context of structured light scanning, an array of coarse to fine fringe patterns are projected on the object's surface acting as a series of planes intersections, reducing the number of individual scans required when compared to the laser-based methods. This also reduces the need for mobile elements

required in the sweeping motion of laser scanners.

Because these 3D scanning methods are based on optical properties, they are known to be sensitive to ambient light, object color and surface finish (Jiang et al., 2012). To limit the impact of ambient light, academic studies and modern commercial 3D scanners commonly project blue light instead of white and equip the camera lenses with an appropriate filter to filter out parasite light wavelengths (Jiang et al., 2012). The scanning of metallic parts is particularly complex because of their reflectiveness (Ross et al., 2011). Finish altering techniques such as painting, and powder deposition must be considered (Palousek et al., 2015). Moreover, the variation in reflectiveness of a surface, which is a typical trait of machined and shot peen-formed parts, leads to missing data and introduces the need for a point cloud consolidation method such as the one proposed in (Liu et al., 2011).

In the case of in-process measurements, such as required by a closed-loop, accuracy is not the only limiting factor. Since the measurements from two different process iterations need to be compared to identify the progression of the process, the repeatability of measurements constitutes the principal limiting factor. For such applications, understandably, a less accurate but repeatable method will provide comparable sets of measurements, but with limited error reduction. On the other hand, an accurate method that lacks repeatability is unusable for in-process measurements. Besides the inherent limitations of each measurement method, further uncertainty is introduced by the data processing required to interpret the measurements. Most methods base their measurements on an intrinsic frame of reference. To be able to compare the measurement data with simulation data, it needs to be translated into the simulation frame of reference. This process known as registration is a necessary part of the post-processing of measurement data and it introduces uncertainty. Therefore, it is not sufficient for the measurement method to be accurate and repeatable, all the subsequent processing steps require the same level or repeatability to guaranty the integrity of the com-

parison. For example, the information provided by an accurate and repeatable structured light 3D scanner can be compromised by less repeatable manual or automated cleaning and cropping of the data. This additional source of uncertainty needs to be considered. On the other hand, conducting all measurements on a CMM using the same measurement grid and frame of reference maintains the repeatability of the measurements.

2.7 Automation of shot peen forming

An automated process involves the execution of its required tasks without or with limited human involvement. The availability of planning methods and nozzle-equipped industrial robots could be considered the only prerequisites for the development of automated shot peen forming. Once a plan is made, a robot can be programmed to execute it to peen form a plate, based on a plan generated by the available planning method. This is feasible in the current state of the shot peen forming industry. However, this form of automation, known as open-loop automation, lacks the notion of precision that sensitive aerospace manufacturing applications require. Further inspection of the formed part would be required. As mentioned in Section 2.1, the inspection of peen-formed parts is at the time a manual process that requires part-specific jigs which are used as references by an operator to measure deviations (Ramati et al., 1999). The complete automation of shot peen forming would therefore require the automation of the inspection of the part and the reformulation of the forming plan based on the measurements. With the measurement methods described in Section 2.6, this is now feasible. This form of automation is known as closed-loop automation. Unfortunately, the literature on shot peen forming automation and especially closed-loop automation is sparse. This can be explained by the competitive industrial value of such a solution and the amount of resource normally required to establish an automated closed-loop shot peen forming system. From a few industrial articles that date to the end of the 1990s and the beginning of the 2000s (Friese et al., 2002; Wüstefeld et al., 2006; Friese, 2006), we have limited insight

on the level of automation implemented in industry. Most notably, the automated shot peen forming company KSA displays hints of closed-loop automation with numerically controlled measurements (Wüstefeld et al., 2006). Although this evidence is limited and the details of the implementation are not publicly available, it can be considered that closed-loop automated shot peen forming has been implemented in industry.

An alternative closer to the current state of the shot peen forming industry would involve a hybrid automation scheme in which a human operator interacts with the shot peen forming robot to perform manual adjustments based on the operator's empirical experience. In this scheme, the robot would handle the physical tasks of the process, while the human agent would focus on the decision-making. This solution would yield part of the benefits of automation in removing the physical strain from the human body but would lack the increased error reduction and the improved repeatability. This notion brings into focus the idea of human-robot interaction and the impact of automation on life (Hentout et al., 2019). Even when considering closed-loop automation, it is important to point out that the human operator is not taken out of the equation at this point. Human experts are always required to supervise the tasks to make sure that the final process is adequate. The idea of closed-loop automation is to augment the capacities of human agents by integrating robotic and numerical tools in areas in which they are better, e.g. lifting heavy weights and performing mechanical simulations. Although the hybrid automation scheme seems an interesting intermediary step towards full industrial automation, it falls in the field of collaborative robotics (Hentout et al., 2019) and falls out of the current scope of this work. It is also valid to point out that this collaborative solution is not mentioned in the shot peen forming literature though it presents a viable solution for the current industrial needs.

The automation of shot peen forming comes with further challenges in terms of control of the process itself. Since the effect of the process is transmitted through random impacts

of projectiles, ensuring the precision of the treated region is non-trivial. The use of small diameter nozzles and media for detailed treatment can be an option, but limits the resolution of the pattern to the nozzle size, as proposed in the context of Fine Particle Shot Peening (Oguri, 2011), and the shot peening of small holes (Barker, 2001). Furthermore, to ensure a constant and stable process intensity, the flow of shot needs to be in a steady state, which demands the jet to be started and left idle until the flow has stabilized. This is typically done outside of the part to prevent the over exposition of a single region of the sample. This introduces further complexities for peening patterns requiring non-continuous paths. Furthermore, complex robot paths with changes in direction imply acceleration and deceleration of the robot, which implies a change in exposure time of certain regions to the shot stream. This would introduce more fluctuation in the shot peening effectiveness on the sample. Accidental impacts on critical regions that were to be kept from treatment can further introduce forming errors or damage critical functional features, such as plate edges and mounting holes. Mechanical deflection of the shot stream is a likely viable solution (Friese, 2006) which has been implemented in industry to block the projectiles from impacting certain regions of the part. Figure 2.6 presents such a deflection apparatus. This solution is reminiscent of the operator's strategy of closing the nozzle with their hand until the desired moment. It needs to be noted that such a solution is viable only in the case where the deflection hardware can close rapidly enough for the shot to be deflected away from the sample and not deflected to a different region of the sample. Such a timing error could lead to more peen forming errors. Alternatively, masking is widely used in the industry to protect sensitive areas of workpieces (Barker, 2001; Faucheux, 2019; Kirk, 1999). Faucheux (2019) demonstrated that complex patterns can be imposed on a part using hand-cut duct tape. This solution decouples the resolution and precision of the pattern from the motion of the peening robot. It also simplifies the robot tool path to only require a uniform coverage of the plate surface in a zig-zag path, leaving the task of enforcing the pattern to the mask. On the other hand, this method's repeatability is limited by the manual operations required, which can be solved through au-

tomation. The removal of the tape after treatment can deform thin samples, introducing errors. A solution to precisely and repeatably control the application of the peening pattern is required to truly automate the process.

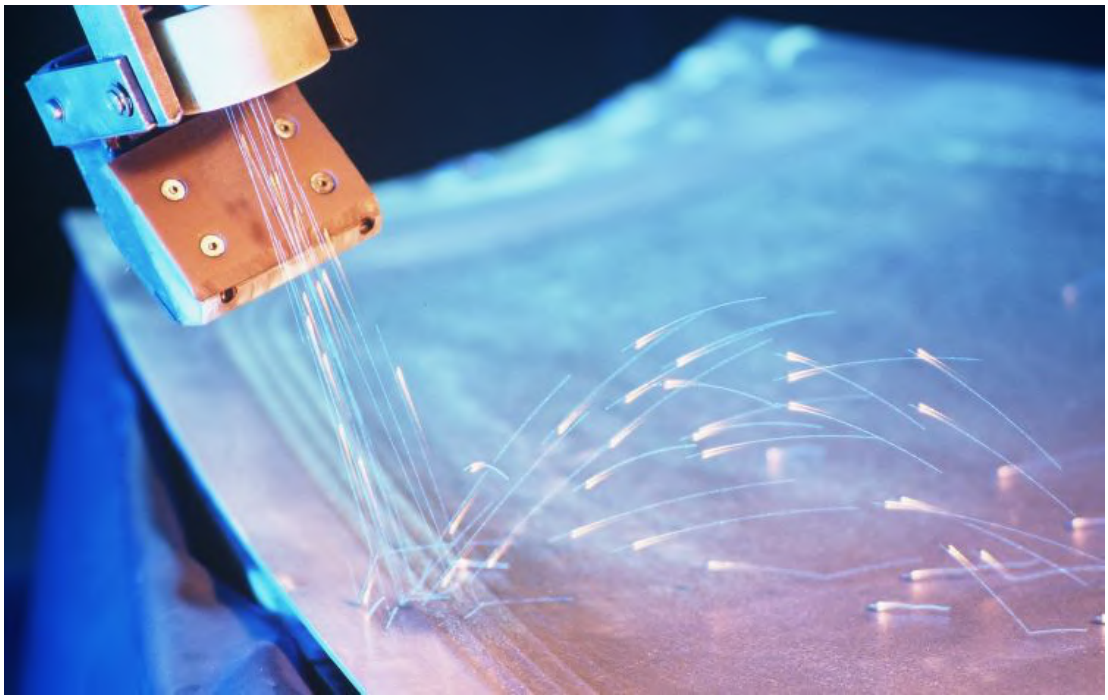

Figure 2.6 Numerically controlled flaps block and allow the shot to impact the part to provide an automated control of the impacted zones. Reproduced with permission from KSA (Copyright KSA).

Along with the precise control of the treatment positions, the intensity of the process involves control challenges. Since the process intensity depends on the media and its impact velocity, the use of multiple intensities in a single forming iteration is non trivial. Certain industrial systems (Friese, 2006) offer the possibility to easily change between media. The use of separate peening systems with different intensity settings is a viable solution, but far from economical. For the sake of repeatability, changing the air pressure driving the nozzle during a forming iteration would involve precise control over the inlet pressure. Nguyen et al. (2021) proposed a controller to regulate the inlet pressure to obtain the desired peening intensity, validated with a model comparing inlet and nozzle pressures. A more conventional

approach using masks would involve the computation of patterns for each intensity, fabricating the corresponding masks and performing a peening iteration for each prescribed intensity.

Since all parts contain initial residual stress as mentioned in Section 2.5, and that in-process stress measurement is at the time impractical, an alternative is to compensate for the measured shape error with a closed-loop. In a sense, the human shot peen forming operator performs a closed-loop. The operator learns how the material behaves, not by measuring the residual stresses left by the process, but by observing the changes in the shape of the component and adapting their actions to these observations. Instead of relying on expert knowledge and human intuition, an automated closed-loop needs to rely on models and sensor data to adapt. As presented in Section 2.3, models to simulate both the local and global effects of shot peen forming are available in the literature. Some of these models also lead to the creation of derived planning methods presented in Section 2.4. Suitable methods to measure the shape of peen-formed plates are available both in the literature and as commercially available solutions as presented in Section 2.6. With these methods, data regarding the forming error with respect to the desired target geometry can be estimated. The remaining aspect to enable an automated closed-loop is not currently covered in the shot peen forming literature. This missing link is the ability to connect the measured data to the planning model to compute a correction plan. Without this part of the loop, the measurement data can only enlighten us to the committed error without the ability to correct it. This is acceptable in the case of pure evaluation of the performance of a simulation or planning method, but insufficient for closed-loop automation. This topic is further addressed in Chapter 6 in which a method to transfer the measured error to the planning method is proposed.

CHAPTER 3 OBJECTIVES AND RATIONALE

The principal objective of this thesis is to develop a method to automate shot peen forming in a closed-loop using in-process measurements. As described in Section 2.7, the literature on closed-loop shot peen forming is sparse, while a few hints of industrial implementations of automated shot peen forming are available. On the other hand, the literature provides references for detailed implementations of simulation and planning tools that can be leveraged towards automation. Planning the shot peen forming problem requires solving a non-linear problem which implies executing iterative mechanical simulations. Additionally, the simulation and planning tools provided by the literature lack the means to compensate for in-process errors that have been linked to initial residual stresses in parts as presented in Section 2.5. The fact that methods to measure residual stresses are either expensive or destructive prohibits their in-process use. To bypass this limitation a closed-loop scheme can be considered to compensate for measured errors through in-process re-planning. However, the literature lacks a method to link measured errors with planning a algorithm.

Along with the motivating needs listed above, this thesis was further motivated by a series of technical opportunities. The advances in machine learning have rendered deep learning frameworks more available and offer solutions for solving complex non-linear problems in real-time. The advances in metrology now offer accurate and repeatable methods for in-process shape measurement. Finally, the availability of low-cost components stimulated by the development of the 3D printing field offers the possibility to design tailored robotic systems. These low-cost automated systems offer the opportunity to simplify the infrastructures required for development and testing.

Based on these observations, we can define the objectives of the thesis as the following.

- Develop a planning method for shot peen forming without computationally expensive in-process iterations.
- Develop a method to update a planning model with measured shape error, to compute a correction plan.
- Automate shot peen forming in closed-loop with in-process measurements.

The result of each stated objective is presented in the following chapters. Chapter 4 presents a neural network able to plan shot peen forming in real-time, when trained on finite element simulation data. The neural network proposed in the chapter could be used in future works as part of a Deep Reinforcement Learning framework to iteratively plan, form and adapt to the resulting deformation measured in a sample. However, the current thesis deviates from machine learning in Chapter 6 to revisit optimization-based planning, with the idea to extend currently available planning methods for closed-loop shot peen forming. Chapter 5 presents a detailed design of an open-source shot peen forming system leveraged in the automated shot peen forming presented in this work. Chapter 6 finally presents the optimization-based closed-loop shot peen forming method developed in this work. The chapter contains an experimental test case which demonstrates that the presented method can considerably reduce the initial forming error for three tested samples.

CHAPTER 4 ARTICLE 1: EFFICIENT PLANNING OF PEEN-FORMING PATTERNS VIA ARTIFICIAL NEURAL NETWORKS

Wassime Siguerdidjane, Farbod Khameneifar, Frédérick P. Gosselin

Published in the Manufacturing Letters journal in August 2020

Abstract

Robust automation of the shot peen forming process demands a closed-loop feedback in which a suitable treatment pattern needs to be found in real-time for each treatment iteration. In this work, we present a method for finding the peen-forming patterns, based on a neural network (NN), which learns the nonlinear function that relates a given target shape (input) to its optimal peening pattern (output), from data generated by finite element simulations. The trained NN yields patterns with an average binary accuracy of 98.8% with respect to the ground truth in microseconds.

4.1 Introduction

The performance of artificial neural networks has been proven on visual pattern recognition tasks (Krizhevsky et al., 2012). Here, we demonstrate that the inverse problem of shot peen forming, consisting in finding a suitable treatment, can be formulated as a visual pattern recognition problem, and accurately and efficiently solved using a neural network.

Peen forming is the process of shaping thin metal parts by bombarding them with a stream of shot at high velocity. Treating certain regions of a part gives rise to local curvature, without expensive geometry-specific tools, such as dies and matrices. This process is frequently used in the aerospace industry to correct distortion in machined parts and to form large panels such as wing skins (Kulkarni et al., 1981).

The final deformed shape of the part depends on the treated regions, referred to as the peening pattern. To select the peening pattern, today's industry mostly relies on human intuition with operators trained in this craft with a qualitative understanding of the mechanics through trial and error. This is time-consuming, inaccurate and expensive.

Predictive models are crucial to predict the outcome of a planned peening pattern. Different modelling approaches have been proposed for peen forming (Xiao et al., 2019a; VanLuchene and Cramer, 1996; Gariépy et al., 2011). Notably, Faucheux et al. (2018) proposed the bilayer framework. Figure 4.1 depicts how the cumulative effect of multiple shot impacts induce surface compressive residual stresses, which in turn result in the local expansion of the treated shallow portion of the plate. Combining the treated expanded layer with the unaffected bottom layer forms a curved bilayer. Thermal expansion efficiently models the effect of the treatment, and is readily available in most finite element software. Adjusting the thermal expansion coefficient and the thickness of the active layer controls the intensity of the process.

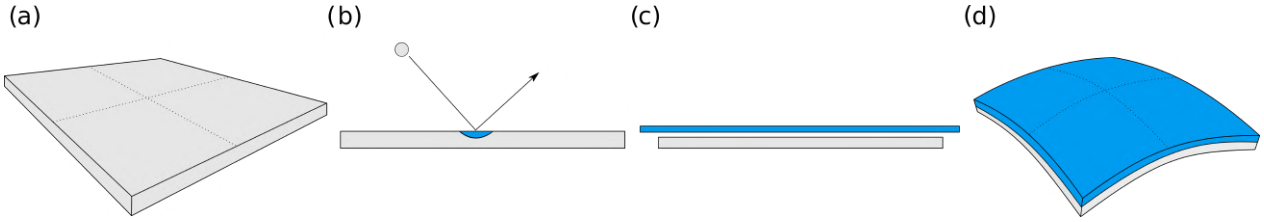

Figure 4.1 Representing the mechanics of peen forming as a bilayer plate problem: (a) Initially flat plate; (b) Visualization of the local effect of an impact; (c) Multiple impacts expand the upper portion of the plate, while the rest of the plate is unaffected, causing a geometrical incompatibility; (d) Final deformed plate uniformly treated. Inspired by Faucheux (2019)

The shape of real peen-formed parts still deviates from the model's predicted shape, mainly due to unknown initial residual stresses in parts (Faucheux, 2019). Since the measurement of residual stresses is either expensive or destructive (Schajer, 2013), a potential solution is to adjust the model using feedback during the process. The long-term objective of our research is to maximize the robustness of automated peen-forming by incorporating modelling and 3D shape measurement in the control loop for adaptive adjustment of the model with the

feedback from shape measurement during peen forming.

The bilayer framework efficiently simulates the deformed shape when applying a peening pattern, i.e., the direct problem. However, the inverse problem can only be solved through iterative optimization. The difficulty is that the direct problem should be solved in every iteration of the optimization, which makes it inefficient to solve the inverse problem. For closed-loop process control, the inverse problem needs to be solved for each treatment iteration. The development of a more efficient method for real-time process planning is therefore necessary.

Here we demonstrate that with the bilayer framework, predicting the peening treatment to form a flat plate into a target shape can be formulated as a pattern recognition problem, solvable with a trained neural network with sufficient accuracy, while only requiring a computation time of the order of microseconds.

4.2 Theoretical Background on Neural Networks

Neural Networks (NNs) are nonlinear function approximators optimized through gradient-based methods to fit a given dataset. NNs learn to predict the most probable output given the training data provided. They learn from known references (ground truths). The conventional training framework requires the dataset to be separated into a training set to optimize the network's parameters, a validation set to validate and tune the network's hyper-parameters, such as the network's depth and learning rate, and an isolated test set to evaluate the network's performance on unseen data. This training framework ensures that the model is not overfitting the training data (Goodfellow et al., 2016).

4.3 Methodology

We propose to train a NN on data generated with the Finite Element Method (FEM) based on the bilayer framework (Faucheux et al., 2018). The objective of this NN is to predict

the required peening pattern, when given a map of the average Gaussian curvature of each element.

Fig. 2 shows the data generation pipeline. 60,000 examples were generated. 40,000 examples were used for training the NN, while 10,000 were used for validation. The remaining 10,000 examples from the dataset served to test the final performance of the model.

Since symmetry conditions are applied during the simulation, only a quarter of the plate is considered. The program generates the training patterns by initially creating random maze images of the size of a quarter of the plate (Fig. 2a) using the depth-first search algorithm (Cormen et al., 2009) (adapted from (Greig, 2016)). The A^* search algorithm (Cormen et al., 2009) (adapted from (Lifszyc, 2013)) then finds a path within the maze to navigate the workpiece from one randomly selected point to another, hence creating a random continuous path (Fig. 2b). The path is then widened by recursively padding it with one pixel on each side. This operation ensures that the generated pattern is larger than a single pixel, which corresponds to the resolution of the mesh. This work assumes that the considered peen forming patterns would be experimentally enforced through the use of shot peening masks, and therefore are not limited by the diameter of the nozzle. All pixels on the generated path are assigned a value of 1 representing the requirement of treatment (blue pixels in Fig. 2c). Fig. 2d presents the final pattern image after being symmetrized to cover the full plate. The generation of these random patterns offers a diversity of continuous shapes that span the surface of the plate, to represent arbitrary reachable peen forming cases.

The open-source FEM software CalculiX (Dhondt, 2004) then computes the deformed shape (Fig. 2f) of the initially flat plate with a static analysis considering geometric non-linearities. The pattern is applied on the plate at a single time to represent the use of a mask. The bilayer model considers a real plate treated in the same way to be held flat during the peen forming process, and released to observe the deformation induced by the treatment.

The square plate of size $L \times L \times h$ (32 mm $\times$ 32 mm $\times$ 1 mm) is discretized on a grid of

32x32 S8R elements. These elements define a composite of two layers: the active top layer of thickness $h_{active} = 0.1$ mm with a positive thermal expansion coefficient α, and the passive bottom layer of thickness $h_{passive} = 0.9$ mm, which is unattainable by the treatment. A constant temperature $T = 1$ °C is applied. Increasing the α value of the treated elements applies the load on the plate. This simulates a bi-axial expansion $\epsilon = \alpha T$ in the active layer of the treated elements. This study considered $1.36\text{e}{-2} \leq \alpha \leq 1.09\text{e}{-1}$ °C^{-1}. As in Ref. (Faucheux et al., 2018), the dimensionless bending moment generated by the expansion of the active layer is defined as

$$\Gamma = 6\,(1+\nu)\,\epsilon \frac{h_{active} h_{passive} L^2}{h^4} \tag{4.1}$$

where $\nu = 0.33$ is the Poisson coefficient of the material of the plate. The process-oriented interpretation of Γ defines the dimensionless peening intensity.

Since the peen forming effect is predominantly bending, curvature is selected as an efficient representation of the plate deformation rather than nodal deflection. The Gaussian curvature is computed at each node of the mesh with the Gauss-Bonnet theorem implemented in the python library PyMesh (Zhou, 2018), and then averaged for each element. This shapes the data as two images of the same size, encoding respectively the target shape (Fig. 2f) and its corresponding pattern (Fig. 2d). The neural network takes as input the target curvature map and outputs the most probable peening pattern to reach it. The output pixel values correspond to the probability that an element should be treated, based on the statistical distribution of training data.

Although a convolutional neural network (Lecun et al., 1998) would have been an alternative, this work demonstrates that the simpler multilayer perceptron (MLP) is adequate for the current task. The number of elements in the plate mesh defines the width of the proposed six-layer MLP (Van Der Malsburg, 1986). The images in the dataset are flattened into vectors to be passed to the MLP. The model is implemented with Keras 2.2.4 (Chollet et al., 2015) and

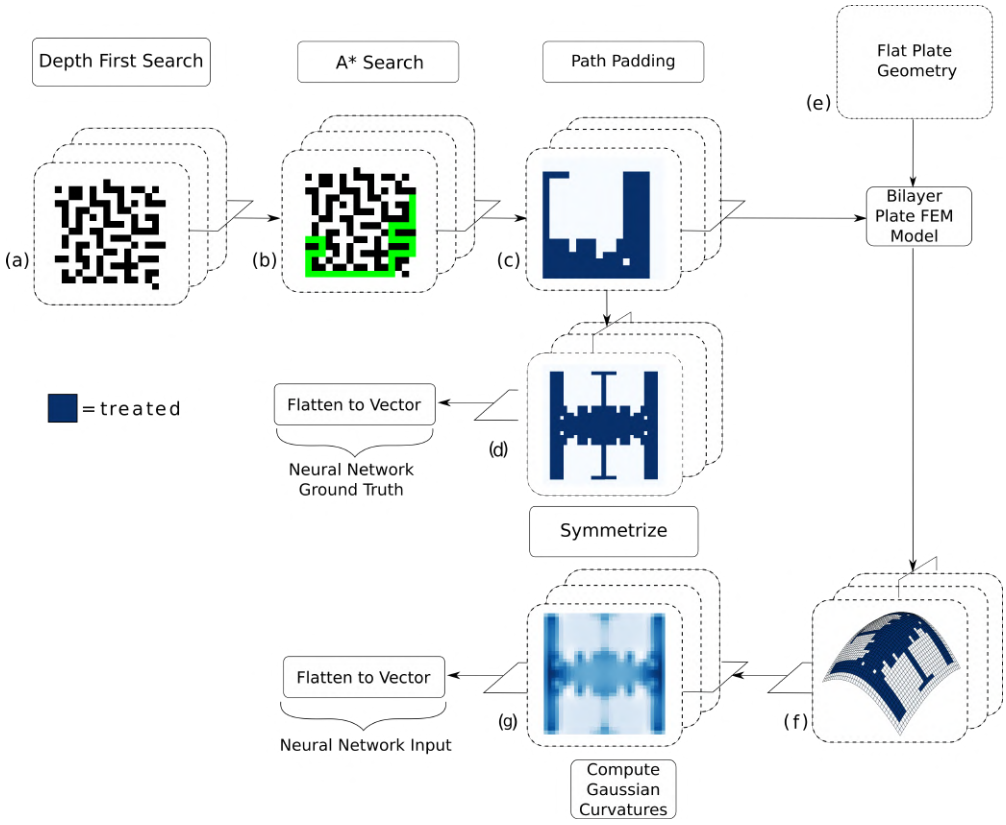

Figure 4.2 Data generation pipeline: (a) Random maze image where each pixel represents an element of the FEM; (b) Continuous path in the maze found by the A^* search algorithm; (c) Resulting peening pattern after path padding operations used to widen the peening area. This pattern covers a quarter of the plate, since symmetry conditions are leveraged in the FEM simulation; (d) The final pattern image used as ground truth, after being symmetrized to cover the full plate; (e) Initially flat mesh of a quarter of the plate; (f) Deformed mesh resulting from the FEM bilayer simulation using the generated peening pattern; (g) Gaussian curvature image.

Tensorflow 1.12.0 (Abadi et al., 2015) as backend. Batch Normalization (Ioffe and Szegedy, 2015) is applied to every layer. A grid search led to the model hyper-parameters selection (Fig. 3). The Adam optimizer (Kingma and Ba, 2014) executed the training. Backpropagation algorithm (Rumelhart et al., 1986) minimized the mean squared error (MSE) loss function between the predicted patterns and the known reference patterns, until the training loss and validation loss converged (Figure 4.3). The MSE loss function was chosen empirically by comparing its performance with other loss functions such as cross-entropy.

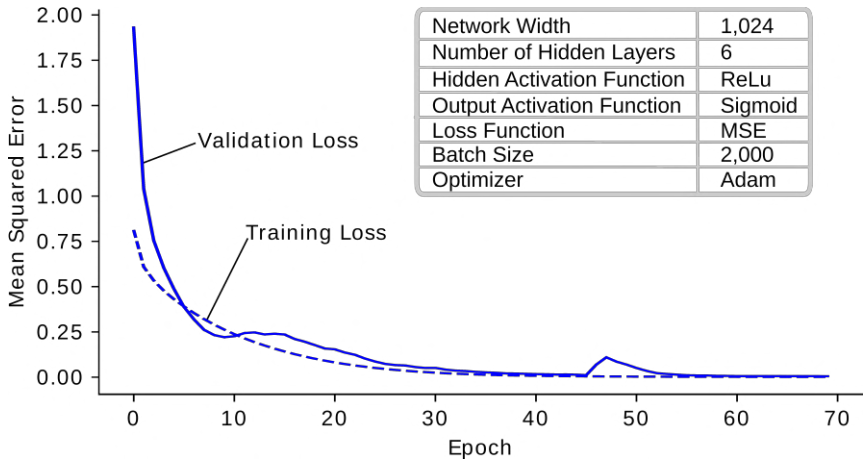

Figure 4.3 Learning curve and hyper-parameters.

4.4 Results and Discussion

The data generation took 20 hours, and the model training took 15 minutes. The prediction time of the model only takes 45 microseconds. This last value is crucial when considering the application of this model to a real-time process. The development and the evaluation of the model were conducted on a laptop computer with an Intel® Core™ i7-6700HQ CPU, with 16GB of RAM and under the Ubuntu 18.04 operating system. Graphics Processing Unit (GPU) acceleration was not leveraged in this study.

The presented results were computed on a test set of 10,000 examples simulated with $\Gamma = 20$. Figure 4.4a shows that the binary accuracy evaluated on the test set averages 98.8%. This accuracy metric is widely used for image classification, and in this context it represents the percentage of elements correctly classified. Figure 4.4b shows that the majority of the test examples exhibit a MSE close to zero.

The Hausdorff distance (Taha and Hanbury, 2015) computed between the mesh nodes of the deformed plate under the peening pattern produced by the NN and the reference peening pattern measures the deviation of the resulting shape from the target shape. Both meshes are defined in the same simulation reference frame, with the centre node at the origin. Normalizing this distance by the diagonal of the mesh bounding box offers a dimensionless metric

proportional to the size of the deformed plate. Figure 4.4c shows the distribution of the normalized Hausdorff distance for the test set. It further demonstrates the performance of the model, with an average of 0.02%. Figure 4.4d presents the normalized confusion matrix computed on the test set. It shows that the percentages of false positives and false negatives are small. These results are complemented with a satisfactory F1-score of 0.981.

Figure 4.4e shows a sample of the best and worst cases of patterns predicted by the NN as compared to ground truth for a given input Gaussian curvature.

The relationship between the applied peening intensity and the simulated curvature of the plate is non-linear. For a uniformly peened square plate, at low intensity ($\Gamma < 20$) it adopts a spherical deformation, whereas at high intensity ($\Gamma > 20$) it adopts a cylindrical deformation (Faucheux et al., 2018). We thus check how the ability of the NN to predict the right pattern is affected by the peening intensity. To do so, we train the NN four times with four datasets obtained at four peening intensities. During this process, the hyper-parameters and network architecture remain unchanged. Figure 4.4f represents the distribution of binary accuracy for various peening intensities (i.e., different values of dimensionless bending moment Γ). Overall, the accuracy decreases slightly with the increase in the peening intensity, but remains high even for very large intensities. All instances of the neural network converged to a low loss value, without exhibiting signs of overfitting.

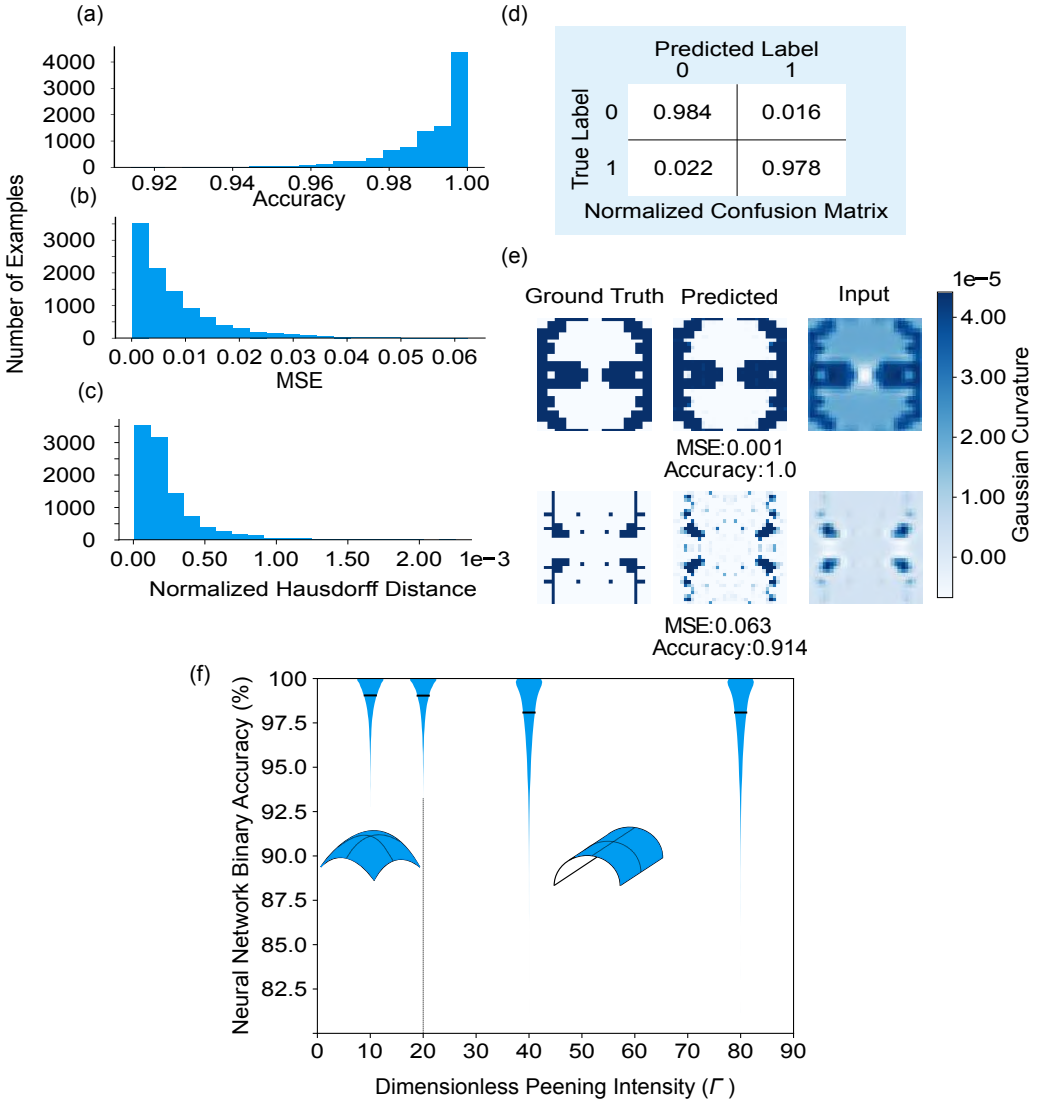

Figure 4.4 Distribution of (a) binary accuracy and (b) mean squared error over the test set; (c) Distribution of Hausdorff distance in the test set, normalized by the mesh bounding box diagonal. The fact that (a),(b) and (c) show high accuracy, low MSE and low Hausdorff distance for all test set examples, validates the generalization of the model beyond the training set; (d) The normalized confusion matrix demonstrates the presence of small percentages of false negatives and false positives; (e) A random selection of the best and worst examples from the test set, presenting the ground truth reference (left), the predicted pattern (middle), and the input Gaussian curvature image (right); (f) With the increase of intensity, the plates are proven to deform in a cylindrical mode, rather than spherical (Faucheux et al., 2018). The violin plot presents the distribution of the test set binary accuracy for various dimensionless peening intensities, with highlighted mean values. We observe a slight increase in the accuracy standard deviation in the cylindrical domain.

4.5 Conclusion and outlook

The main contribution of this work is the demonstration that the inverse problem of peen forming can be represented as a visual pattern recognition problem, by encoding the geometry of the target shape in terms of Gaussian curvature. This approach solves the problem via a neural network, a proven technique for pattern recognition tasks.

The limitations of this model lie in the need for a large dataset that represents the various possible target shapes that can be achieved using a given treatment intensity. Proving the generalization of such model on any possible shape is an open problem.

This work constitutes the first step towards the long-term goal of developing closed-loop peen forming by incorporating neural networks and the feedback provided by the geometric inspection data from a 3D scanner to compensate for deviations caused by unknown residual stresses in peen formed parts. The data-driven nature and differentiability of NNs are the central features that demonstrate their potential to adapt to new examples, therefore, correct their prediction errors based on new data.

Since our developed method makes use of the bilayer framework, it would easily be adaptable to a broad range of problems which can also be simulated with bilayers such as biological growth (van Rees et al., 2017; Haas et al., 2020), active materials (An et al., 2018) or solvent absorption (Pezzulla et al., 2016).

Acknowledgements

This work was funded by Aerosphere Inc., the Fonds de recherche du Québec – Nature et technologies and the ministère de l'Économie, de la Science et de l'Innovation [Funding reference number LU-210888].

CHAPTER 5 ARTICLE 2: A LOW-COST OPEN-SOURCE AUTOMATED SHOT PEEN FORMING SYSTEM

Wassime Siguerdidjane, Farbod Khameneifar, Frédérick P. Gosselin

Submitted to the HardwareX journal in October 2021

Abstract

The aerospace industry relies on shot peen forming to form sheet metal parts and correct distortion in machined parts. The shot peen forming community is developing simulation and planning methods to meet the industrial need for automation. Researchers need to invest in expensive industrial robots contained in large blasting cabinets to perform the experimental validations of their proposed methods. To bypass this need for expensive industrial-grade equipment, this work presents a low-cost shot peen forming system that enables researchers to validate their methods experimentally on small samples. Conventional installations can cost a few 100,000 USD while the proposed prototype only costs 400 USD to produce. Such a prototype can operate on a tabletop with conventional electrical installations. The use of small samples for validation further reduces the cost of experiments and allows for faster development.

5.1 Hardware in context

Shot peen forming is a cold working process used in the aerospace industry to form large sheet metal panels. It leverages high-velocity impacts to induce compressive residual stresses in the material. These stresses lead to changes in the curvatures of the part. The industrial and academic implementations of the process in automated conditions usually demand industrial robots with large blasting cabinets. These solutions are expensive and require large

spaces. While 6-axis industrial robots offer the possibility to work on complex geometries, most academic research in the field is conducted on simple plates (Faucheux et al., 2018; Gariépy et al., 2013; Grasty and Andrew, 1996; Miao et al., 2021; Siguerdidjane et al., 2020) to validate proposed modelling and process planning solutions. This suggests that a simpler solution may be considered by most researchers in the field. In this article, we propose a low-cost open-source shot peen forming robot able to form small samples. The presented prototype was leveraged to validate experimentally our closed-loop automation scheme for shot peen forming.

5.2 Hardware description

The peening system is a 2-axis cartesian robot made from 2020 aluminum extrusions, powered by stepper motors and controlled by an Arduino Mega microcontroller with the Ramps1.4 shield, running the Marlin 3D printer firmware. The peening task is handled by a sand-blasting nozzle fixed on the robot's gantry, that projects the blasting media on the sample. The robot itself is housed in a plastic storage container to keep the media inside and make it reusable. This solution provides a table-top alternative to the standard solution of using an industrial robot arm housed in a blasting cabinet. The other main advantage to the proposed solution is the cost reduction, the peening robot costs about 400 USD, while industrial infrastructures usually involve a few 100 000 USD. Additionally, this solution lets the user choose the software with which the system interacts without license limitations or black box implementations. This is particularly interesting in the context of academic research since researchers usually want control over their hardware and software. Since the robot is controlled by an open-source 3D printer firmware, the user is free to modify it as required and the robot supports serial command transmission in the form of G-code. The solution is constructed out of a majority of off-the-shelf components and a few 3D printed parts, making it easy to replicate. Figure 5.1 presents a photograph of the proposed peen forming system.

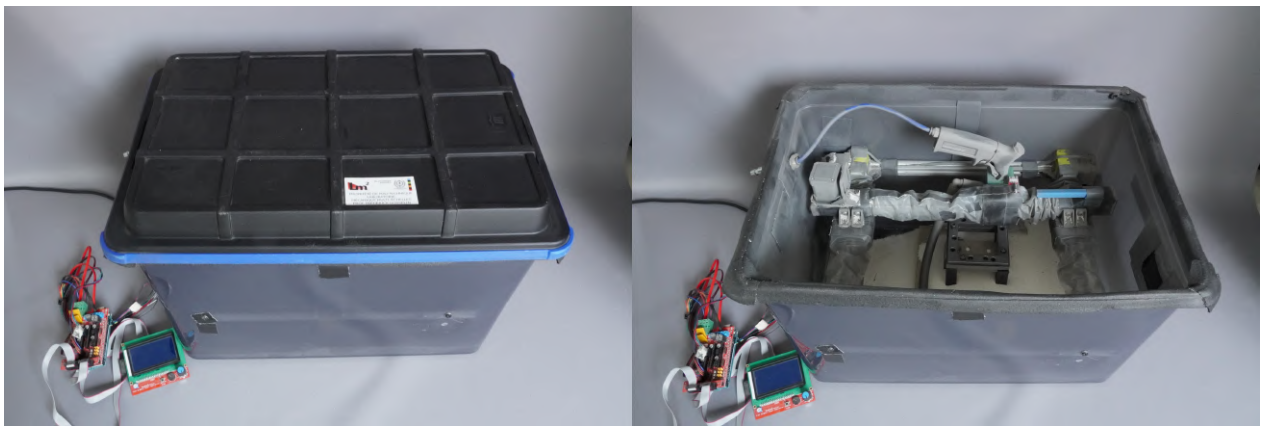

Figure 5.1 Photos of the shot peen forming system presenting the lid of the container on and off.

The presented hardware can be useful for users interested to:

- Perform in-house automated small scale shot peen forming of plates at low cost
- Perform automated sandblasting finishing on parts

5.3 Design files

The design files are available in the project repository at `https://osf.io/z5rvn/`, along with a G-code file sample to control the robot. The designed parts are all 3D printed using PLA. These parts serve to support drive components and protect the components, such as the rails, wheels and pulleys from the shot media. If not properly shielded from the shot, these components will either be damaged over time or their functions will be impaired during operation.

5.3.1 Design Files Summary

Table 5.1 presents the required design files. All parts in the design files table are 3D printed using PLA filament.

1. cover_motor_x.FCStd: a part covering the stepper motor shaft and the drive pulley for the x-axis. It provides a rigid covering to keep the flexible rail cover from interfering with the drive;

2. belt_cover_x.FCStd: a part covering the belt and idler pulley for the x-axis. It also provides a rigid covering of the components;

3. cover_center_x.FCStd: a part covering the x-axis gantry. It provides a rigid covering of the gantry and keeps the flexible rail cover from tangling in the wheels;

4. cover_motor_y.FCStd: a part covering the stepper motor shaft and the drive pulley for the y-axis. It provides a rigid covering to keep the flexible rail cover from interfering with the drive;

5. belt_cover_y.FCStd: a part covering the belt and idler pulley for the y-axis. It also provides a rigid covering of the components;

6. cover_center_y.FCStd: a part covering the y-axis gantry. It provides a rigid covering of the gantry and keeps the flexible rail cover from tangling in the wheels;

7. sandblaster_mnt.FCStd: a part used to mount the sandblasting nozzle to the gantry.

Table 5.1 Design file table

Design filename	File type	Open source license	Location of the file
cover_motor_x.FCStd	CAD	GNU GPL v. 3	https://osf.io/z5rvn/
belt_cover_x.FCStd	CAD	GNU GPL v. 3	https://osf.io/z5rvn/
cover_center_x.FCStd	CAD	GNU GPL v. 3	https://osf.io/z5rvn/
cover_motor_y.FCStd	CAD	GNU GPL v. 3	https://osf.io/z5rvn/
belt_cover_y.FCStd	CAD	GNU GPL v. 3	https://osf.io/z5rvn/
cover_center_y.FCStd	CAD	GNU GPL v. 3	https://osf.io/z5rvn/
sandblaster_mnt.FCStd	CAD	GNU GPL v. 3	https://osf.io/z5rvn/
sandblaster_cover.FCStd	CAD	GNU GPL v. 3	https://osf.io/z5rvn/
belt_bearing_support.FCStd	CAD	GNU GPL v. 3	https://osf.io/z5rvn/

8. sandblaster_cover.FCStd: a part used to secure the sandblasting nozzle to the sandblasting mount.

9. belt_bearing_support.FCStd: a part used to support the idler pulley.

5.4 Bill of materials (BOM)

This section presents the off-the-shelf parts and materials required to build the presented shot peen forming robot. Table 5.2 summarizes the parts and costs of the mechanical assembly, while table 5.3 summarizes the electronic parts required as well as their cost. It details the number of parts required for the build as well as the number of parts in each package in which the component can be purchased at the location listed in the detailed BOM linked in the project repository. To stay concise, the suggested locations for purchase are only listed in the detailed file on the repository.

Table 5.2 Mechanical bill of materials (For more detail refer to the csv file available in the repository at `https://osf.io/z5rvn/`).

Component	Qt./build	Qt./pkg	cost/pkg	Qt. of pkg	Cost (USD)
M5X8 screw	18	10	$0.99	2	$1.98
M5X10 screw	10	10	$1.09	1	$1.09
M5X15 screw	3	10	$1.19	1	$1.19
M5X20 screw	3	10	$1.29	1	$1.29
M5X30 screw	2	10	$1.49	1	$1.49
M5X45 screw	4	10	$1.79	1	$1.79
M3X10 screw	8	1	$0.29	8	$2.32
M4X12 screw	5	100	$9.86	1	$9.86
M5 nut	13	100	$1.76	1	$1.76
M5 washer	16	100	$3.14	1	$3.14
M4 nut	5	100	$1.41	1	$1.41
M4 washer	5	100	$2.86	1	$2.86
4 hole L bracket	4	12	$10.45	1	$10.45
4 hole straight bracket	2	20	$13.67	1	$13.67
Mini V gantry	3	1	$34.99	3	$104.97
2020 v-slot 500mm	5	1	$5.49	5	$27.45
Nema 17 mounting bracket	3	4	$12.38	1	$12.38
Corner bracket	8	20	$10.72	1	$10.72
M5 t-nuts	24	100	$13.67	1	$13.67
GT2 belt kit	1	1	$20.11	1	$20.11
1/4NPT quick-connect fitting	1	1	$4.42	1	$4.42
1/4NPT push fitting	2	10	$27.23	1	$27.23
1/4 inch OD PTFE tube	1	1	$11.21	1	$11.21
Sandblaster	1	1	$20.91	1	$20.91
Plastic storage bin	1	1	$17.04	1	$17.04
Total					**$324.41**

Table 5.3 Electrical bill of materials (For more detail refer to the csv file available in the repository at `https://osf.io/z5rvn/`).

Component	Quantity	Cost per unit	Cost (USD)
Arduino Mega RAMPS kit	1	$50.48	$50.48
12V solenoid valve	1	$13.90	$13.90
12V 5A power supply	1	$10.68	$10.68
Arduino relay module	1	$7.23	$7.23
Grounded power chord	1	$11.02	$11.02
Total			**$93.31**

5.5 Build instructions

5.5.1 General instructions

The mechanical build is separated into sub-assemblies, which are then assembled to form the complete build. The electrical wiring instructions follow the mechanical build instructions. Figure 5.2 presents a rendered representation of the global mechanical drive assembly of the robot. This provides the reader a general idea of the assembly before the build instructions of each sub-assembly are presented.

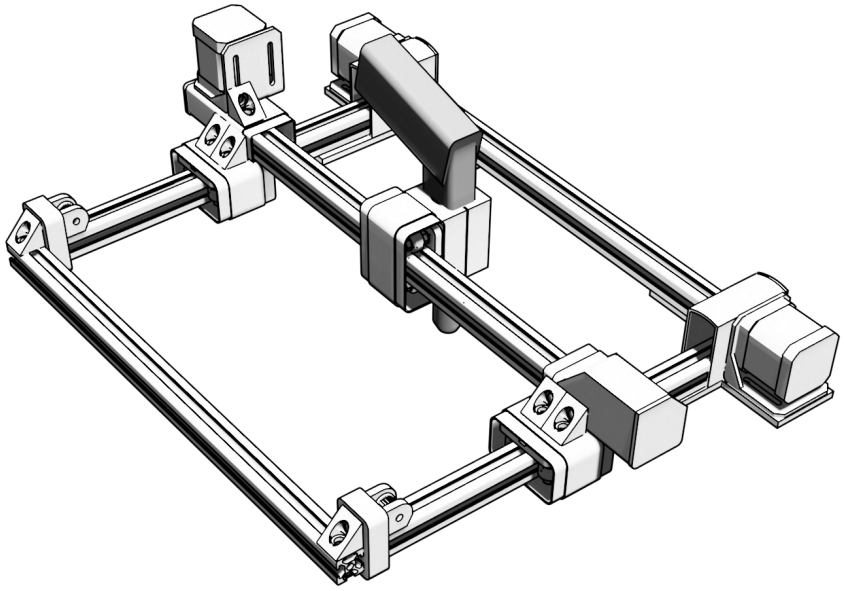

Figure 5.2 Rendered representation of the global mechanical drive assembly of the robot.

The 2020 extrusions can be cut to the desired length to accommodate the available storage bin. If the reader prefers to build a custom enclosure for the robot, it is also possible, though it was not considered necessary for the purposes of the project.

5.5.2 X-axis motor sub-assembly

This section describes the assembly of the X-axis motor sub-assembly. Figure 5.3 presents an exploded view of the sub-assembly.

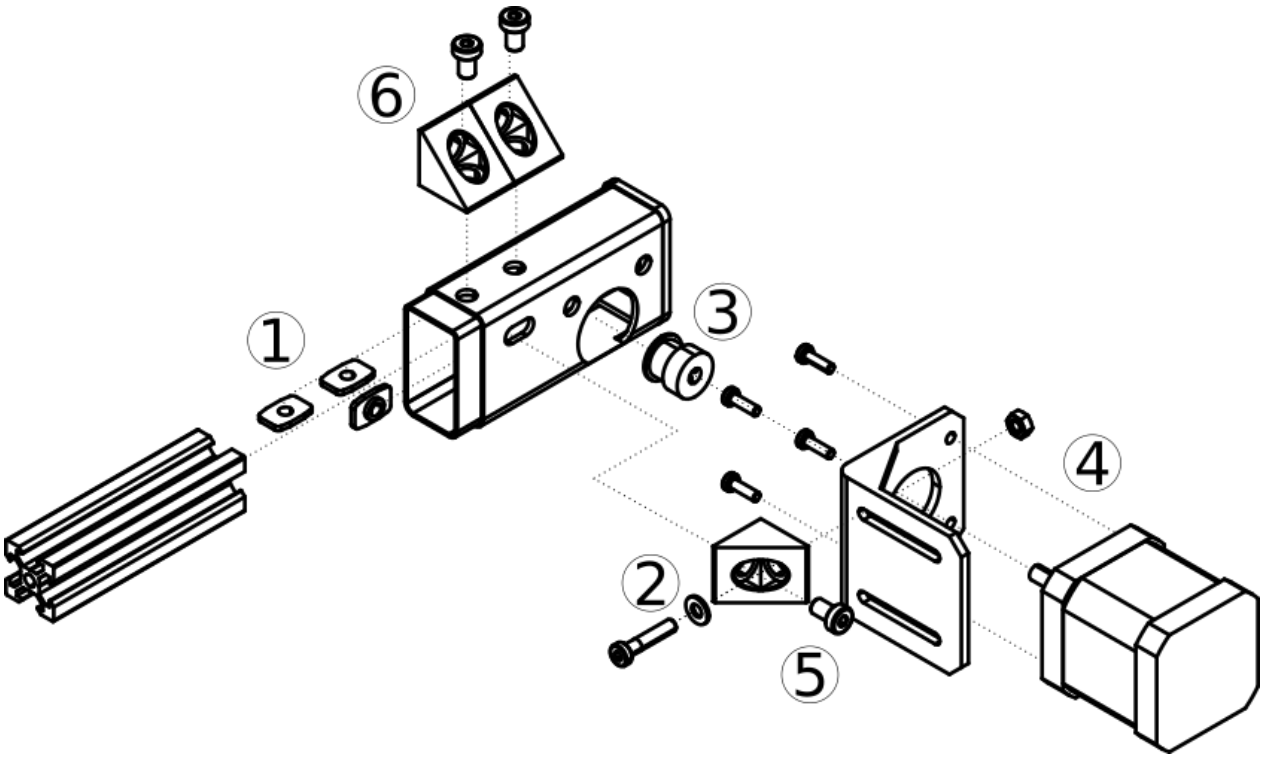

Figure 5.3 X-axis motor sub-assembly.

1. Insert 3 t-nuts on the x-axis 2020 extrusion, as shown on Figure 5.3;
2. Mount a first corner bracket to the Nema 17 bracket using an M4X12 screw, an M4 washer, and an M4 nut;
3. Mount a GT2 drive pulley to the Nema 17 shaft. Secure the pulley with the included set screws;
4. Mount a Nema 17 stepper motor to the Nema 17 bracket with 4 M3X10 screws;
5. Thread an M3X8mm screw through the first corner bracket, the x-axis motor cover,

and into the lone t-nut (Figure 5.3). This step secures the motor to the extrusion and the cover;

6. Join two corner brackets to the motor cover and 2020 extrusion by threading two M3X8mm screws into the two remaining t-nuts. These two corner brackets will join the x-axis to the y-axis gantries.

5.5.3 X-axis gantry sub-assembly

This section describes the assembly of the X-axis gantry sub-assembly. Figure 5.4 presents an exploded view of the sub-assembly.

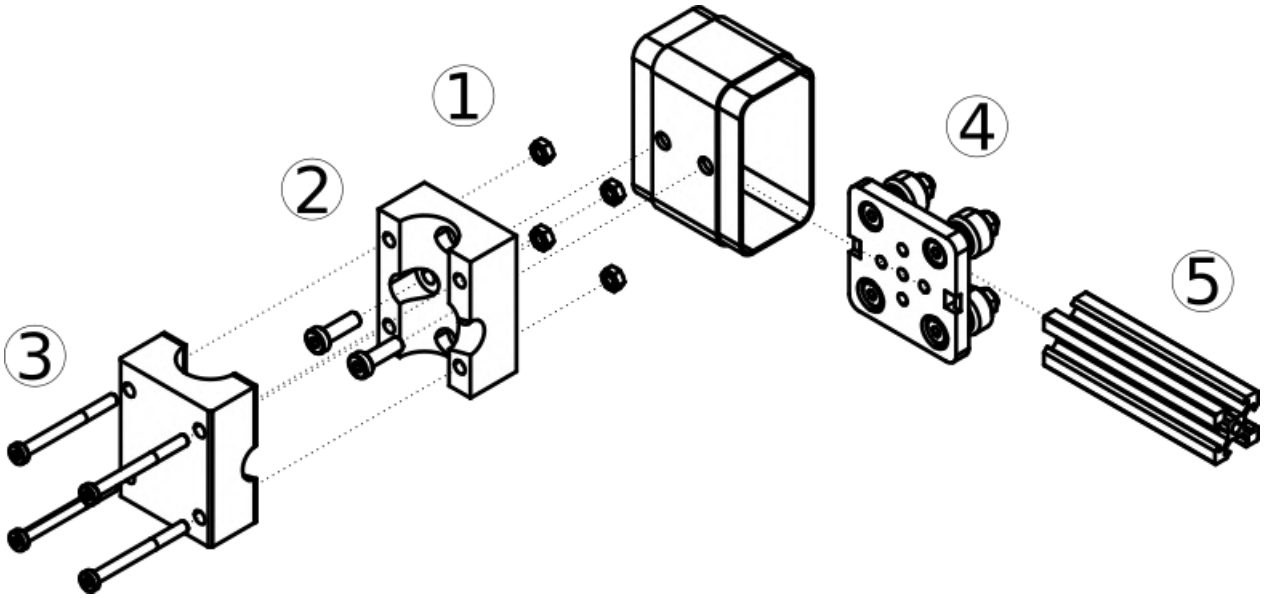

Figure 5.4 X-axis gantry sub-assembly.

1. Insert 4 M5 nuts in the sandblaster mount (Figure 5.4);

2. Mount the sandblaster mount and gantry cover to the Openbuild mini V gantry using two M5X16mm screws threaded into the mini V gantry;

3. The sandblaster is secured by screwing the sandblaster mount cover to the sandblaster mount with 4 M5X45mm screws;

4. Loop the GT2 belt around the notches available on the mini V gantry. This belt will loop around the X-axis motor drive pulley and the X-axis idler pulley to provide drive to the x-axis gantry;

5. The X-axis gantry sub-assembly then slides on the x-axis 2020 extrusion.

5.5.4 X-axis idler pulley sub-assembly

This section describes the assembly of the X-axis idler pulley sub-assembly. Figure 5.5 presents an exploded view of the sub-assembly.

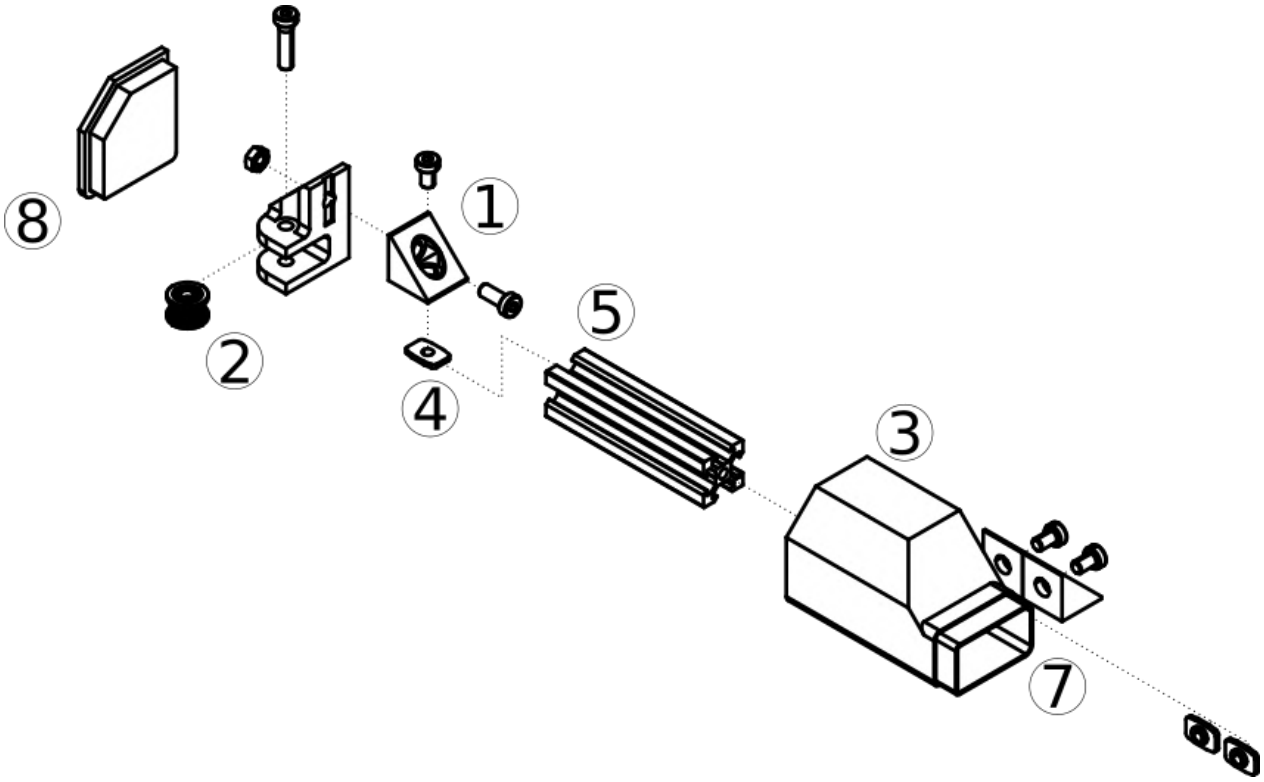

Figure 5.5 X-axis idler pulley sub-assembly.

1. Mount a corner bracket to the idler pulley mount, using an M5X16mm screw and an M5 nut (Figure 5.5);

2. Mount the idler pulley to the idler pulley mount with an M5X20mm screw threaded into the mount;

3. Slide the idler assembly cover on the X-axis 2020 extrusion;

4. Insert two M5 t-nuts in the X-axis 2020 extrusion;

5. Mount the corner bracket to the X-axis 2020 extrusion with an M5X8mm screw and an M5 t-nut;

6. Loop the X-axis drive belt around the idler pulley and fix it to the X-axis gantry;

7. Slide the cover over the idler assembly and fasten it and two corner brackets to the 2020 extrusion with two M5X8mm screws and M5 t-nuts. The two corner brackets will be used to connect this portion of the X-axis to the Y-axis gantry, similarly to the corner brackets of the motor cover assembly;

8. Cap the idler pulley assembly cover with its lid. The lid and the cover are printed with an interference fit, but for further sealing, silicone rubber caulking can be applied to the joint.

5.5.5 Y-axis motor sub-assembly

This section describes the assembly of the Y-axis motor sub-assembly. Figure 5.6 presents an exploded view of the sub-assembly. Two instances of this sub-assembly are necessary. These steps need to be followed for the right and left Y-axis assemblies.

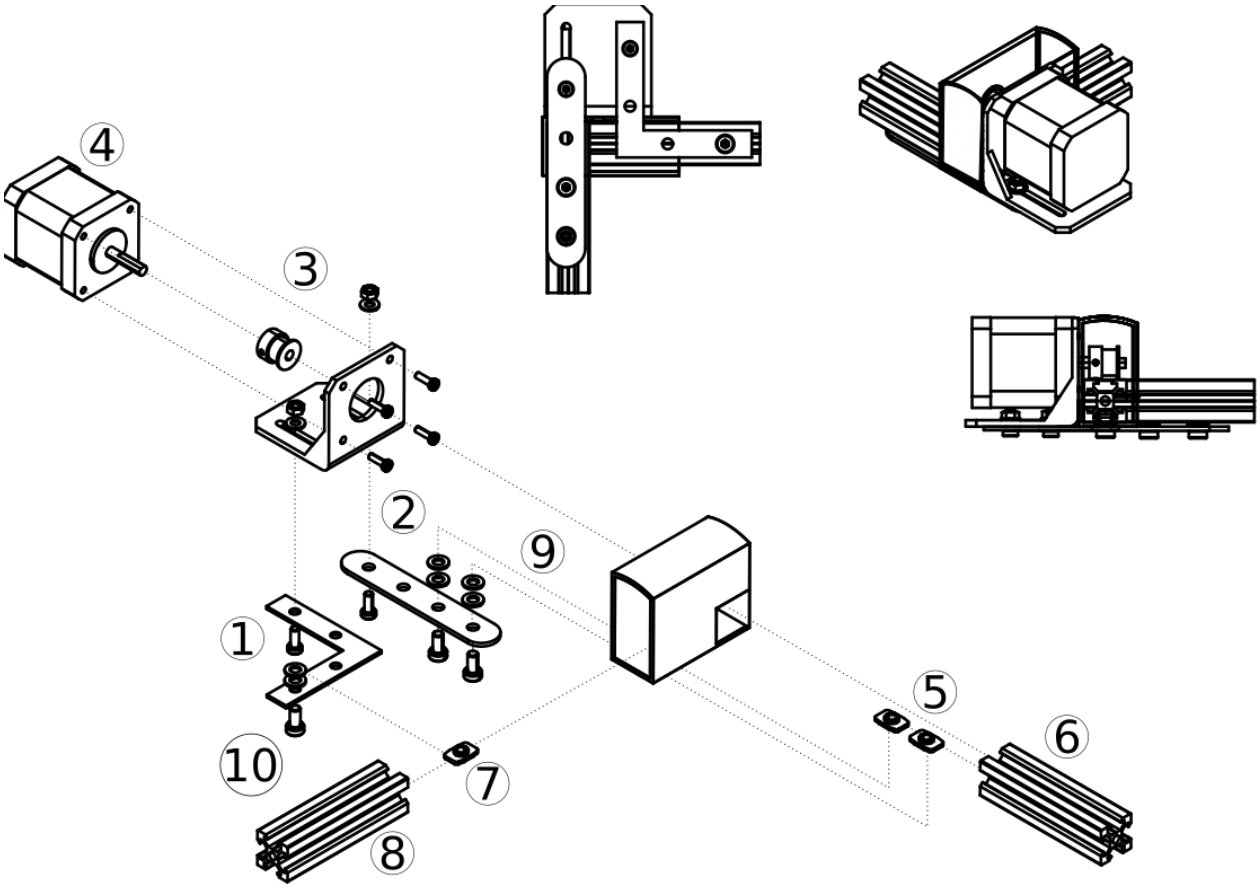

Figure 5.6 Y-axis motor sub-assembly.

1. Mount the L-bracket to one slot of the Nema 17 bracket as shown in Figure 5.6, using an M4X12mm screw, an M4 washer, and an M4 nut;

2. Mount the straight flat bracket to the other slot Nema 17 bracket as shown in Figure 5.6, using an M4X12mm screw, an M4 washer, and an M4 nut;

3. Mount a GT2 drive pulley to the Nema 17 shaft. Secure the pulley with the included set screws;

4. Mount a Nema 17 stepper motor to the Nema 17 bracket with 4 M3X10 screws;

5. Insert two M5 t-nuts in a 2020 extrusion. This extrusion serves as a structural component, not as an axis rail;

6. Slide the 2020 extrusion in the square hole of the motor cover;
7. Insert an M5 t-nut in one of the Y-axis 2020 extrusions;
8. Slide the motor cover on the Y-axis 2020 extrusion;
9. Mount the straight flat bracket onto the structural 2020 extrusion by treading two M5X10mm screws, through two M5 washers and into the two M5 t-nuts;
10. Mount the L-bracket onto the Y-axis 2020 extrusion by treading an M5X10mm screw, through two M5 washers and into the M5 t-nut;
11. Loop the Y-axis drive belt around the GT2 pulley.

5.5.6 Y-axis gantry sub-assembly

This section describes the assembly of the Y-axis gantry sub-assembly. Figure 5.7 presents an exploded view of the sub-assembly. Two instances of this sub-assembly are necessary. One assembly is fastened to the X-axis idler pulley assembly and the other to the X-axis motor assembly.

1. Loop the Y-axis drive belts to one side of each gantry and fasten them with zip ties;
2. Slide the gantry covers over the Openbuild mini V gantries;
3. Fasten the corner brackets from the X-axis assembly to the Openbuild mini V gantry with two M5X8mm screws through the gantry cover. If assembling the left Y gantry, fasten the brackets of the X-axis idler assembly. For the right assembly, fasten the brackets of the X motor assembly;
4. Slide the gantry assemblies on the Y-axis 2020 extrusions.

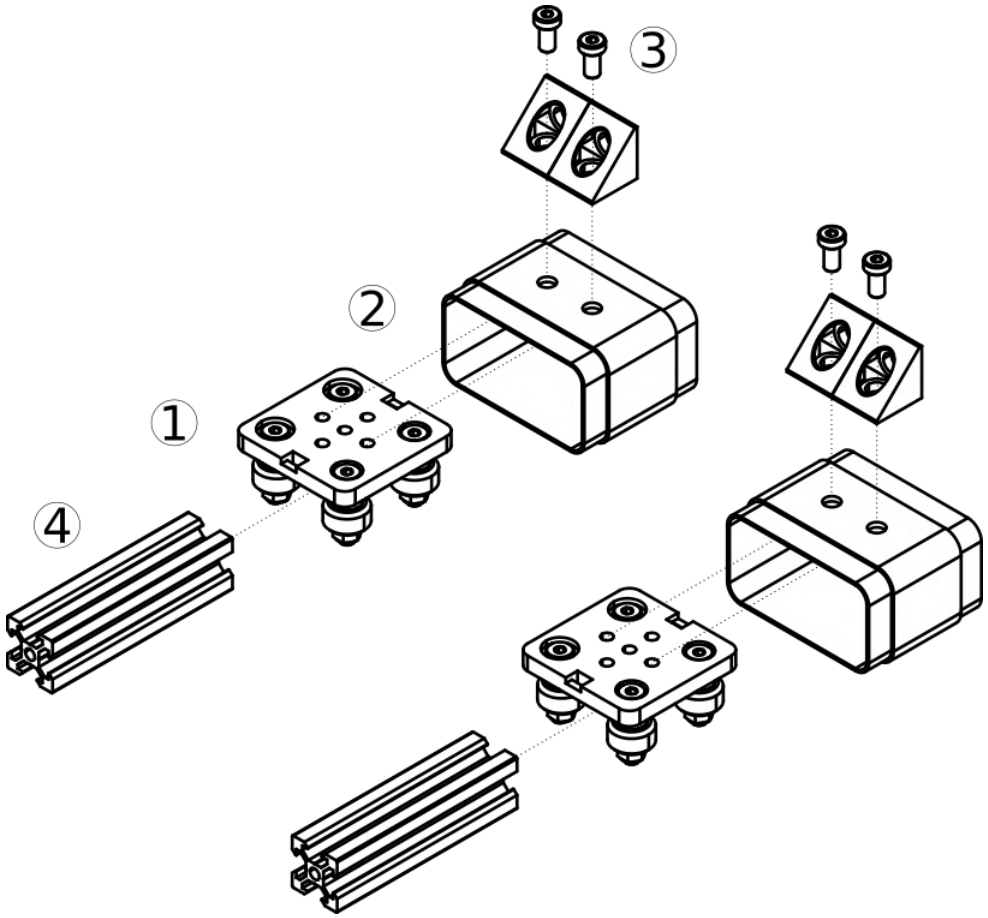

Figure 5.7 Y-axis gantry sub-assembly.

5.5.7 Y-axis idler pulley sub-assembly

This section describes the assembly of the Y-axis idler sub-assembly. Figure 5.8 presents an exploded view of the sub-assembly. Two instances of this sub-assembly are necessary. These steps need to be followed for the right and left Y-axis assemblies.

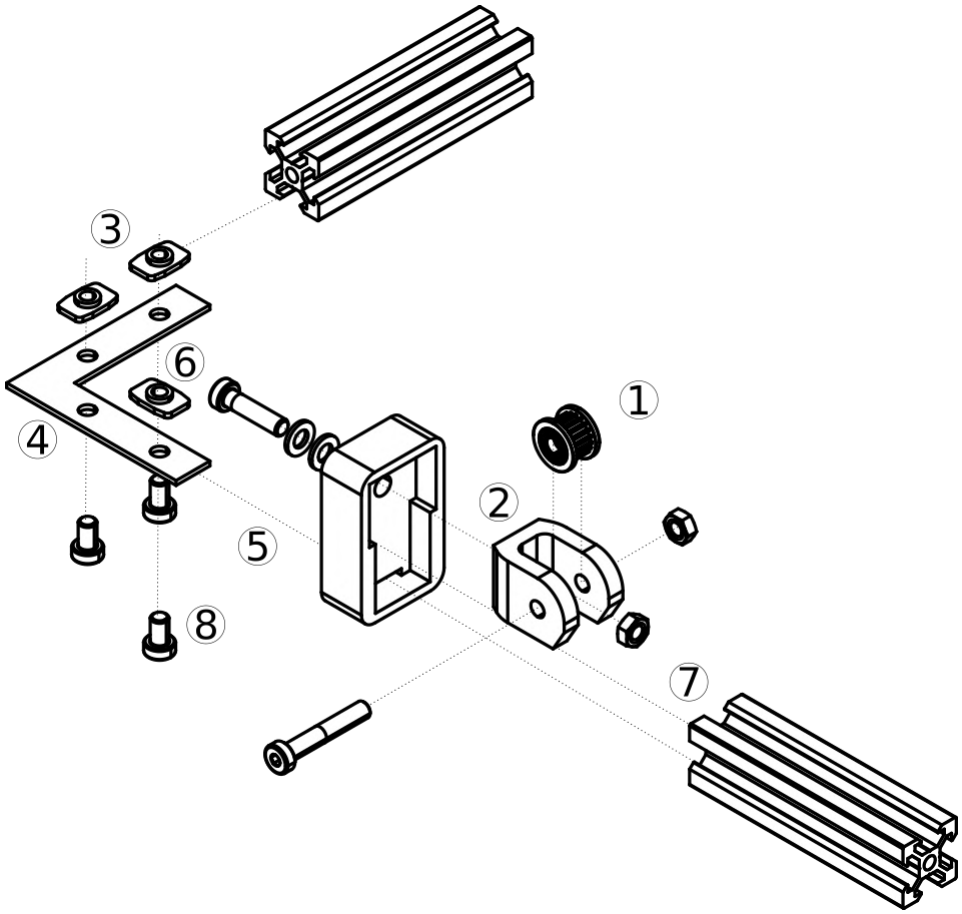

Figure 5.8 Y-axis idler pulley sub-assembly.

1. Mount a GT2 idler pulley to the pulley bracket using an M5X30mm screw and an M5 nut;

2. Mount the pulley bracket to the pulley cover using an M5X20mm screw and an M5 nut;

3. Insert two M5 t-nuts in a 2020 extrusion. This extrusion serves as a structural component, not as an axis rail;

4. Mount the L-bracket to the structural 2020 extrusion by threading two M5X8mm screws into the t-nuts;

5. Slide the L-bracket through the slot in the pulley cover;

6. Insert an M5 t-nut in the Y-axis 2020 extrusion;

7. Slide the Y-axis 2020 extrusion in the pulley cover;
8. Mount the L-bracket to the Y-axis 2020 extrusion by threading an M5X8mm screw into the t-nut;
9. Loop the Y-axis drive belt around the idler pulley and into the belt slot on the gantry.

5.5.8 Mounting the robot motion assembly to the container

This section describes the mounting of the robot motion assembly to the storage container used as housing. Refer to Figure 5.1 for a general view of the assembled robot in its housing.

1. Select the mounting height of the robot for all components to clear the lid when moving. This depends on the chosen storage container;
2. Trace four reference points to drill four holes in the container for mounting;
3. Drill four holes on the marked reference points;
4. Insert two M5 t-nuts in each of the two structural 2020 extrusions;
5. Thread four M5X8mm screws through the mounting holes in the storage container and into the M5 t-nuts.

5.5.9 Sealing and component protection

Shot peen forming generates dust. The goal of the robot housing is to keep most of the generated dust within. All components within the housing will be covered in dust and will be impacted by the projectiles. The rails, if left unprotected, will also accumulate shot media, which will get lodged in the wheels and impede the motion of the robot. This section presents the steps required to seal the robot housing and protect the components housed within it.

1. Adding insulation neoprene foam tape to the lid increases the quality of the seal, reducing the quantity of dust that can escape the housing;

2. The chosen storage bin featured integrated latches to secure the lid to the container. Alternatively, 3D printed latches can be designed for a storage bin that lacks such a feature. Also, binder clips can be used to secure the lid or to enhance the integrated latches for a more even sealing pressure;

3. The rails can be protected with traditional bellows, but in this project, we tested the low-cost alternative of using 4 mil polyethylene sheets. These sheets can be cut and joined with glue or tape, or welded with heat from a soldering iron to make sleeves that are mounted to the 3D printed covers with zip-ties.

5.5.10 Electrical wiring instructions

The instructions take into account that the user is familiar with Arduino microcontrollers. This project leverages an Arduino Mega fitted with a RAMPS 1.4 shield. The setup of the RAMPS shield, in terms of jumper and driver installation, is presented in the RAMPS documentation on the RepRap wiki (RepRap, 2021). The project uses the Marlin firmware to drive the system. The procedure to upload and set up the firmware is standard and detailed in the Marlin documentation (Marlin, 2021). For this project, we use the X and Z axis of the shield only, since only two degrees of freedom are necessary. A more complex 3-axis system could be designed and used for the same shot peen forming purpose, but for treating plates, a simple 2-axis system is sufficient. The motors of the Y-axis of the robot are connected to the Z-axis of the shield because two connection ports are available, with only one available port for the other axes (Figure 5.9). The D9 port (Figure 5.9) is used to control the solenoid valve and is represented in the firmware as a fan, which is a standard Marlin feature.

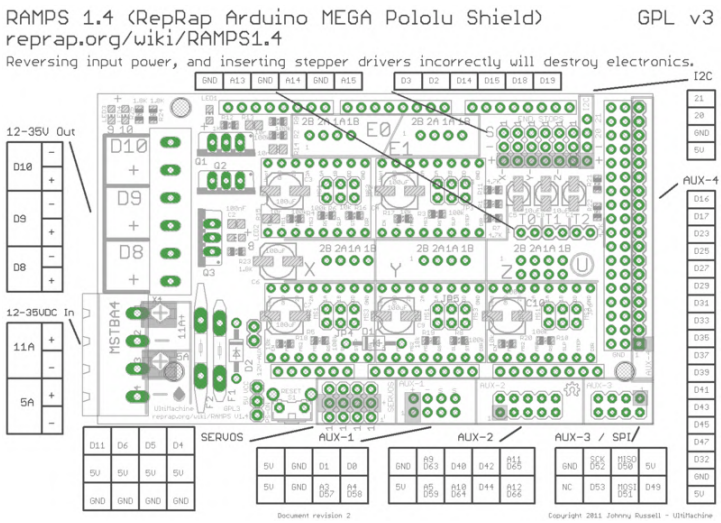

Figure 5.9 RAMPS 1.4 shield layout. Reproduced from (RepRap, 2021).

Figure 5.10 presents a schematic of the wiring required for the project.

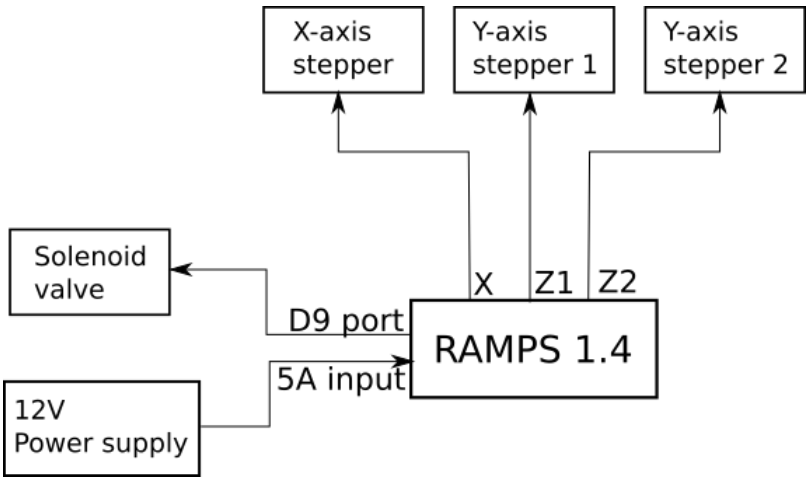

Figure 5.10 Wiring diagram: The 12V power supply is connected to the 5A power input of the RAMPS 1.4 shield. The solenoid valve is connected to the the D9 port of the shield, which provides a 12V output. The stepper motors are connected to their respective ports, as specified by the RAMPS 1.4 documentation (RepRap, 2021).

1. Connect the wires of the 12V solenoid valve to the D9 port on the shield while respecting the polarity;

2. Connect the wires of the X-axis stepper motor to the X motor port on the shield. Upon testing, if the stepper motor rotates in the wrong direction, the orientation of the connection can be flipped;

3. Connect the Y-axis motors to the Z-axis ports on the shield. The Z-axis is used because it provides the ports to connect two motors at once. Therefore, the G-code used to control the robot will be in terms of X and Z motion;

4. Connect the 12V 5A power supply to the 5A port on the shield;

5. Certain power supplies require the user to wire the power plug on terminals (for 110V or 240V). Always use caution when dealing with high voltage and perform the wiring with the power plug removed from the power socket;

6. The user is free to mount the solenoid valve and the power supply to the housing. It is better to keep the microcontroller away from the housing to protect it from potential electrostatic discharges;

7. The microcontroller can be controlled through a USB tether, though we recommend running the G-code using an SD card through a RAMPS display interface. The wiring of such display interface is documented in the RAMPS documentation (RepRap, 2021).

5.6 Operation instructions

5.6.1 Safety

The operation of the shot peening robot requires the following safety considerations:

- Compressors and compressed air are sources of concentrated energy and are dangerous. Never operate compressed air equipment over the manufacturer's pressure rating and make sure that the pressure hoses used are not compromised;

- The cover of the robot housing needs to be closed at all times when the compressed air solenoid is activated;

- Protective goggles are to be worn at all times during the operation of the robot;

- Since the blasting media can generate dust upon impact with the sample, we advise the user to wear a dust mask or a respirator when operating the robot;
- Some blasting media can generate static electricity when passing through the hoses; some minor static shocks are to be expected when touching any conductive surface after handling the robot. Surrounding electronics should be protected against static shocks. For this reason, the Arduino is kept away from the robot housing. The use of rubber gloves will reduce this inconvenience and protect the surrounding electronics from static shock when being handled.

5.6.2 Operation

1. As a safety precaution, make sure that the robot is disconnected from the wall outlet and the air pressure source when preparing the robot for use. Always wear safety goggles when operating the machine.
2. Fill the bottom of the robot housing with your media of choice such as steel shot peening media, ceramic media, walnut shell blasting media, sand, sodium bicarbonate (baking soda), etc. Different media will offer different results in terms of treatment effectiveness or surface finish. Make sure the housing contains enough media to allow the intake hose to be submerged in media during the complete operation. The quantity of media is determined empirically.
3. Place your sample in the appropriate fixture to hold it during the treatment. This fixture depends on the shape of the sample.
4. Plug in the machine and turn on the main power switch. This will start the power supply and power the Arduino Mega. After a few seconds, the Marlin loading screen will appear. Once loaded, Marlin displays the status screen.
5. The robot is controlled via a G-code file that the user should place on an SD card. A

sample G-code file is provided in the project repository. The SD card can be inserted in the reader offered by the display suggested in the electrical BOM in table 5.3.

6. The rotary encoder of the display needs to be pressed to access the menu. The user can navigate the Marlin menu by rotating the encoder and pressing it to make a selection.
7. Close the lid of the robot housing.
8. Connect the intake solenoid valve to your compressed air source. Air should not be free to flow at this point.
9. Navigate to the "Print from SD card" menu of Marlin using the display rotary encoder.
10. Select the G-code file containing the sequence of operations.
11. The sample G-code provided begins by opening the solenoid valve to let the compressed air into the system. Since the wires of the valve are connected to the fan control pins on the Ramps 1.4 shield, Marlin requires the M106 command to activate it.
12. The robot will then begin to follow the motion dictated by the G-code file.
13. Once all motion instructions are completed by the robot, the sample G-code contains an M107 command that closes the solenoid valve, stopping the compressed air flow.
14. As a safety precaution, disconnect the compressed air hose from the solenoid valve.
15. The treated sample can now be retrieved from the fixture.
16. If no further treatment is required, the main power switch can be turned off and the robot can be unplugged.

5.7 Validation and characterization

The current section demonstrates an example of the deflections that are attainable with the shot peen forming robot. The deflection of a shot-peened aluminum plate depends on its size,

the shot media, the location of treated regions, the exposure time, the air pressure, and the air flow rate. The hardware was used in our research work on the automation of shot peen forming with a 5-gallon air compressor which can provide an air flow rate of up to 5 CFM. The presented examples were conducted on two plates of 3" × 3" × 0.041" 6061-T6 aluminum uniformly treated. Both samples were incrementally peened for 2, 4, 6, 8, and 10 passes and measured between each pass. The shot peening media used for these tests was Zirshot Z425 ceramic media. One sample was peened with an air pressure of 50 psi and the other with 75 psi. Figure 5.11 shows the resulting shape of the shot-peened sample. The sample treated at 75 psi is presented on the left, and the sample treated at 50 psi is presented on the right. Figure 5.12 presents the deflections of the samples as a function of the number of peening passes. This demonstrates that the low-cost hardware is able to form deflections of up to 0.0941" on 0.041" thick plates.

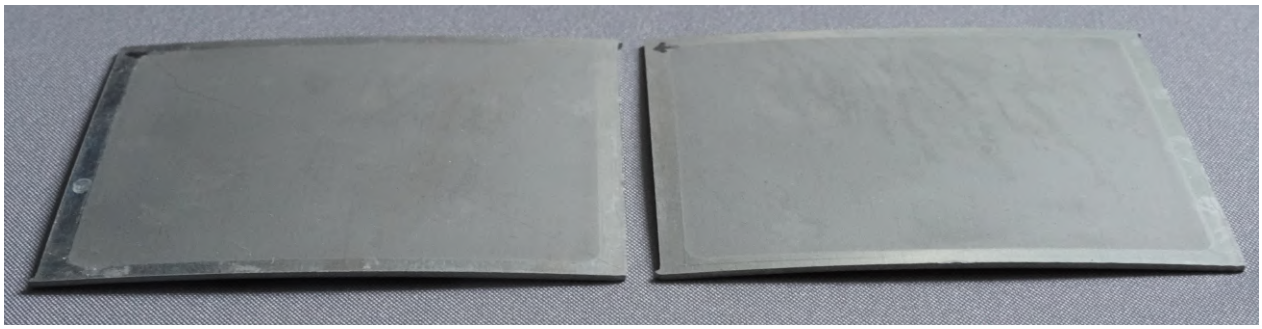

Figure 5.11 The final 3" × 3" × 0.041" shot peened plates after 10 passes, with the 75 psi sample on the left and the 50 psi sample on the right.

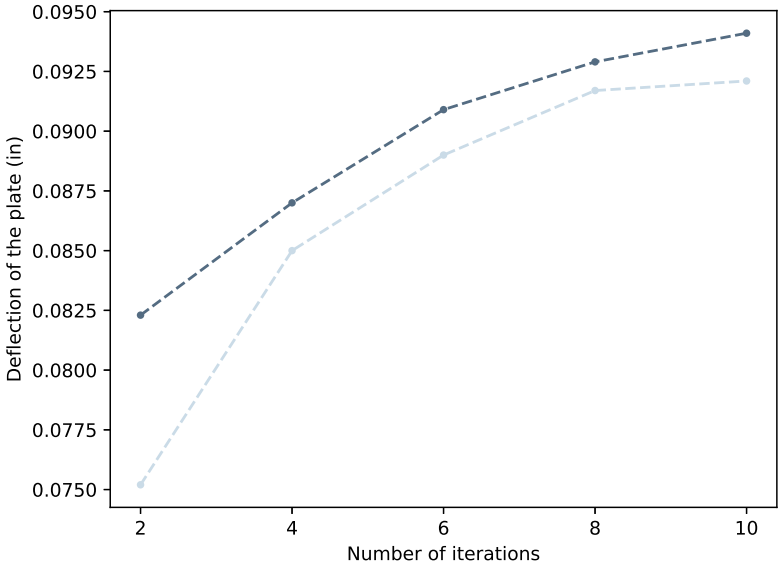

Figure 5.12 The deflection of uniformly peened 3” × 3” × 0.041” 6061-T6 plates as a function of the number of peening passes, for air pressures of 50 and 75 psi with Zirshot Z425 ceramic shot media.

5.8 Acknowledgements

This work was funded by Aerosphere Inc., the Fonds de recherche du Québec – Nature et technologies and the ministère de l’Économie, de la Science et de l’Innovation [Funding reference number LU-210888]. The authors would like to acknowledge the contribution of Tanuj Deshmukh and Jovan Kostenov, who’s internships were centered on the fine-tuning and protection of the hardware.

CHAPTER 6 ARTICLE 3: CLOSED-LOOP SHOT PEEN-FORMING WITH IN-PROCESS MEASUREMENT AND OPTIMIZATION

Wassime Siguerdidjane, Farbod Khameneifar, Frédérick P. Gosselin

Submitted to the Journal of Manufacturing Processes in October 2021

Abstract

Shot peen forming is relied upon in the aerospace manufacturing industry to form thin metal panels into complex geometries. The accuracy and repeatability of the process depend on the initial stress state of the part. The measurement of residual stresses being costly or destructive leaves the field in want of a more efficient method to produce accurate parts. This work proposes a closed-loop method, based on in-process measurements, a finite element model, and optimization to reduce shot peen forming errors by iterative replanning. We demonstrate in an experimental test case of three sample plates that the proposed method can reduce the forming error below 0.2 mm, while the standard open-loop planning yielded errors from 0.333 mm to 0.667 mm, for samples of 1.04 mm thickness.

6.1 Introduction

The aerospace industry relies on the shot peen forming process to form thin metal sheets and correct distortion in machined parts (Kulkarni et al., 1981). The process leverages high-velocity projectile impacts to induce surface compressive residual stresses. These residual stresses expand the affected portion of the material, which bends the plate when constrained by the unaffected portion of the thickness. The use of this process removes the need for expensive part-specific tooling such as dies. Operators rely on empirical knowledge to incrementally form parts, while the industry presents the need for further precision and repeatability

(Wüstefeld et al., 2006). Therefore, the automation of the process presents a growing interest.

Research in the field of shot peen forming offers insight on the modelling of the process in terms of shape prediction (Faucheux et al., 2018; Gariépy et al., 2011; Grasty and Andrew, 1996) and induced stress prediction (Xiao et al., 2019a,b). Modelling tools allow to predict the effect of a specific peening treatment, while industrial applications further require the ability to plan the process, i.e. determine the required process parameters to obtain a desired shape. The process parameters of shot peen forming are defined as the intensity, the coverage and the regions of the part that require peening (Kirk, 2007). We refer to the shape of the treated regions as the peening pattern. Though different approaches have been proposed to plan peen forming (Faucheux, 2019; Luo et al., 2020; VanLuchene and Cramer, 1996; Siguerdidjane et al., 2020), none are able to account for the errors caused by the initial residual stresses and imperfections remnant from the part's forming history (Faucheux, 2019; Gariépy et al., 2013; Schajer, 2013). The available methods to measure these stresses, to explicitly take them into account, are either expensive or destructive (Schajer, 2013).

To bypass this limitation and adapt the process to overcome these sources of error, we propose a closed-loop method that relies on a finite element model (FEM) and optimization to iteratively adjust the process plan based on in-process measurements. Our contribution is threefold: (1) An optimization-based method to explain discrepancies between simulation and observed deflection; (2) integration of this tool in a closed-loop peen forming procedure; and (3) an experimental validation of this procedure. The validation consists of an experimental test case, involving three $76.2 \times 76.2 \times 1.04$ mm 6061-T6 plates to validate the proposed closed-loop scheme. The experiments leverage an in-house small-scale shot peen forming robot to perform the treatment of the samples and an in-house measurement system based on a 3D printer to provide the in-process measurement required for replanning. The design of this shot peen forming robot is detailed in (Siguerdidjane et al., 2021). In this

experimental proof of concept, we demonstrate that the proposed method allows to form flat plates into a given target shape within 0.2 mm of Hausdorff distance (Taha and Hanbury, 2015) with respect to the target, while the initial open-loop planning yields a forming error of 0.333 mm to 0.667 mm.

The rest of the article is structured as follows. Section 6.2 presents the methods and materials, in which the closed-loop scheme is detailed, with its simulation, optimization and experimental shot peen forming workflows. Section 6.3.1 presents the implementation of an experimental test case used to demonstrate the performance of the proposed method. Section 6.3.2 presents the results of the experimental test case. Section 6.3.3 presents a discussion surrounding the proposed method and the presented experimental test case. Section 6.4 concludes the paper.

6.2 Methods and Materials

6.2.1 The bilayer finite element model

This work leverages the bilayer representation of shot peen forming (Faucheux et al., 2018) for all process simulations. Figure 6.1 illustrates the concept of the bilayer model. Figure 6.1a shows an initially flat plate, uniformly treated by multiple impacts in Figure 6.1b. The shot peen forming process affects a shallow depth of the material, depicted as the blue-gray region in Figure 6.1b. The transition between the affected and unaffected portions of material defines a set of two layers, hence a bilayer. The compressive residual stresses induced by the multiple impacts involved in the treatment, force the expansion of the affected layer, as portrayed in Figure 6.1c. The lack of expansion of the unaffected layer introduces a geometrical incompatibility that bends the plate, as shown in Figure 6.1d. The implementation of this concept follows the method proposed by (Faucheux, 2019; Miao et al., 2021), using a finite element model to simulate the bilayer plate. The program was implemented in Matlab

R2018b with DKT18 triangular elements (Batoz and Dhatt, 1972) arranged in pairs to form square plate elements, and two pairs of elements are superimposed to provide a balanced expansion, free from preferential orientation (Faucheux, 2019; Miao et al., 2021). The loads are represented as isotropic expansions, equivalent to thermal expansions, of the top or bottom layers of the elements and provided to the program as a vector of lengths $2 \times n_{elements}$, where $n_{elements}$ is the number of elements of the FEM mesh. Increasing the value of each layer expansion simulates a more effective treatment. The resolution of the FEM mesh controls the resolution of the computed peening pattern. For a more detailed peening pattern, smaller elements are required, which increases the computational cost. In this study, a 16×16 square element mesh was used. For symmetrical geometries, symmetry boundary conditions can be applied to reduce the computational cost.

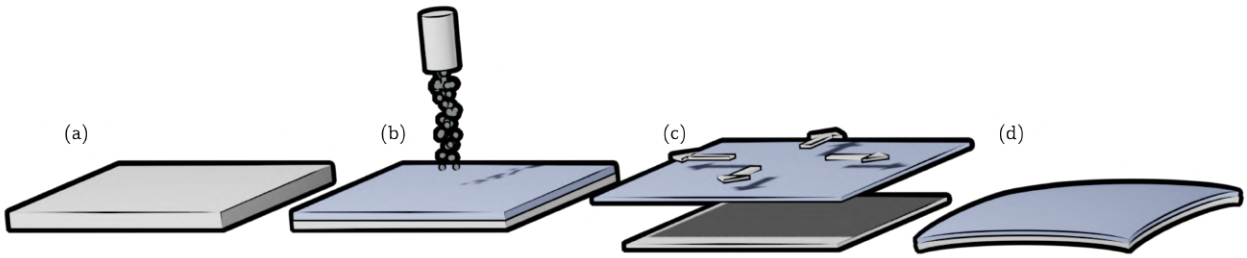

Figure 6.1 The effect of shot peen forming as a bilayer problem: (a) An initially flat plate; (b) multiple impacts affect a portion of the thickness, or active layer; (c) the resulting stresses are observed as an expansion of the active layer; (d) the combination of the expanded layer and the unaffected layer creates a geometrical incompatibility that bends the plate.

6.2.2 Overview of the closed-loop scheme

The proposed closed-loop scheme controls the deformed shape of the plate by iteratively adjusting the peening pattern, while keeping the treatment intensity and coverage constant. The workflow consists of iterations of peening pattern optimization, shot peen forming of the sample, in-process measurements, and correction pattern optimization. Figure 6.2 illustrates the overall process. Figure 6.2a shows a conceptual representation of the optimization of the bilayer FEM (idealized for ease of visualization as a smooth surface) to find the required peening pattern to minimize its deviation in the z-axis with respect to the target shape (represented here as a wireframe). In other terms, this process fits the FEM on the desired target by adjusting the expansions of the top and bottom layers of each element. The result is a peening pattern for the top and bottom face of the plate that is shown in the form of masks in Figure 6.2b. These masks impose the shape of the computed pattern during the treatment, by blocking the areas not to be treated and letting the shot hit the plate where peening is required. This lets the peening nozzle path (e.g., the zig-zag path shown in Figure 6.2c) remain the same for all peening patterns. The deformed plate is then measured (Figure 6.2d) to assess the deviations of the forming process. Figure 6.2e illustrates the second optimization problem which finds the additional expansions that minimize the deviation of the optimized bilayer model with respect to the measurements. We refer to these variables as latent expansions. This work considers the resulting shape of a peen-formed plate as the result of an equilibrium of bending moments induced by the expansions of a bilayer. Therefore, the computed latent expansions represent the unknown variables that balance the expansions induced by the treatment to explain the deviations between the measurements and the shape predicted by the FEM. These expansions provide new bounds to the first optimization problem in Figure 6.2a to account for the observed error, and to compute a correction peening pattern. The next sections detail each step of the loop illustrated in Figure 6.2.

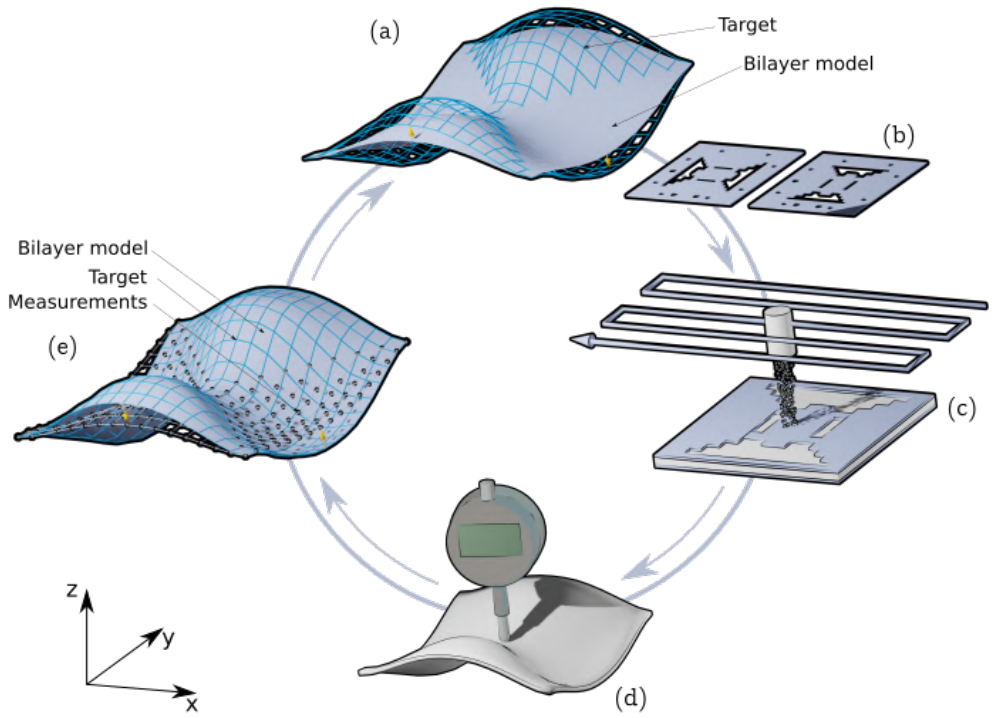

Figure 6.2 Overview of the proposed closed-loop method: (a) The optimization algorithm computes the peening pattern that minimizes the deviation in the z-axis of the bilayer model (solid surface) with respect to the target shape (wireframe). (b) The computed pattern is laser cut in cardstock masks to protect the untreated areas from the shot impacts. (c) The nozzle follows a uniform zig-zag path at a constant speed, and the peening pattern is imposed by the mask. Acceleration and deceleration sequences are conducted outside of the sample. This provides a constant treatment. Both sides are treated. (d) The treated plate is measured. (e) The measurements are used as observations of the effect of the treatment. The optimization algorithm fits the bilayer model to the measured point cloud to estimate the latent expansions responsible for the observed forming error. These latent expansions are given to the optimization algorithm in (a) to compute a correction pattern.

6.2.3 Initial planning optimization

The first optimization problem (Figure 6.2a) has for objective to find the required peening pattern to form the plate into the desired target shape. This step leverages the pattern optimization method proposed by references Faucheux (2019); Miao et al. (2021), in which the interior points algorithm Byrd et al. (1999) finds the distribution of expansions of a bilayer plate FEM, to minimize the mean squared vertical distance with the target shape points. In the context of linear plate mechanics, this optimization problem is convex Faucheux (2019), and therefore a gradient-based optimization algorithm such as interior points is guaranteed

to find the global minimum of the functionBoyd et al. (2004). Similarly to Miao et al. (2021), this optimization problem is defined as:

$$\begin{aligned} \underset{\chi \in R^n}{\text{minimize}} \; & \|z(\mathbf{x}, \mathbf{y}, \chi) - z_{target}(\mathbf{x}, \mathbf{y})\|_2^2 \\ \text{subject to} \;\; & 0 \leq \chi_i \leq 1, \quad i = 1, ..., n \\ & \mathbf{A}^\top \chi \leq A_{max} \end{aligned} \tag{6.1}$$

where $z(\mathbf{x}, \mathbf{y}, \chi)$ refers to the vector of vertical coordinates of the FEM bilayer model, as a function of the vector of expansion χ defining the peening pattern, the vectors $\mathbf{x}$ and $\mathbf{y}$ of node coordinates. The term $z_{target}(\mathbf{x}, \mathbf{y})$ refers to the vector of vertical coordinates of the target shape. The vector $\mathbf{A}$ represents the normalized area of the treated elements and A_{max} is a user-imposed limitation on the total peened area.

This optimization problem is the constrained to force the optimizer to find solutions in which the vector χ only contains values between 0 and 1, to only represent expansions, that are attainable by the shot peening treatment. To represent the true effectiveness of the treatment on the sample, the vector χ is multiplied by an experimentally calibrated expansion magnitude. The process to compute this expansion magnitude is detailed in Section 6.2.4. The second constraint forces the total peened area to be below the user-defined threshold, to prevent the optimizer from producing checkerboard patterns which are viewed as a form of overfit of the target (Faucheux, 2019). A method to define the value of A_{max} is not provided by the authors of the work proposing the optimization method (Faucheux, 2019; Miao et al., 2021). This work has been conducted with a value of $A_{max} = 1.0$, as found in the implementation provided by the author of (Faucheux, 2019). This first part of the process yields comparable patterns as open-loop planning methods currently available in the literature (Faucheux, 2019; Luo et al., 2020; Miao et al., 2021).

6.2.4 Shot peen forming methodology

From this point, the computed pattern is enforced on a sample plate with the use of a mask (Figure 6.2b). In this work, the mask refers to a sheet of 176 g/m^2 card stock, laser cut to enforce the computed pattern and placed on the faces of the plates. The areas to be treated are laser cut out of the mask to let the shot stream impact the surface. In masked areas, the surface is protected from the impacts and therefore not treated. The thickness of the mask depends on the intensity of the treatment, since it needs to provide enough compliance to absorb the impact energy instead of it being transmitted to the sample. This thickness needs to be defined experimentally, by comparing the shape of a sample treated while fully masked with its initial shape. The pattern cut in the mask follows the resolution of the simulation mesh, allowing a direct correspondence between the predicted pattern and the applied pattern. The use of a numerically controlled laser cutter ensures an accuracy and repeatability that could not be matched by manual fabrication of the masks.

Figure 6.3 illustrates a custom jig that registers the masks with respect to the plate, and keeps the latter from deforming during the treatment. The intensity of the treatment is dependent on impact energy transmission from the shot to the plate. A free-to-deform plate will lead to a changing angle of impact, which in turn implies a changing impact energy. According to reference Faucheux (2019), a free to deform plate will exhibit a deformation greater than normally expected for a clamped plate. To ensure a constant and repeatable treatment intensity during the peening process, maintaining the plate flat is necessary. Figure 6.3a depicts the assembled jig, while figures 6.3b and c present it disassembled. Figure 6.3c presents a detailed decomposition of the jig assembly. The jig is comprised of two steel frames (2 & 7) joined by cap screws (1). The frames apply a clamping pressure on the edges of the sample plate (4), while letting the shot contact the interior surface of the plate and mask. This prevents the treatment of the area near the edges of the plate, which is considered in the optimization problem by forcing the expansion of the concerned elements

to zero. Three dowel pins (6) are fixed to the lower steel frame (7) to accurately register both frames, as well as the sample and the masks.

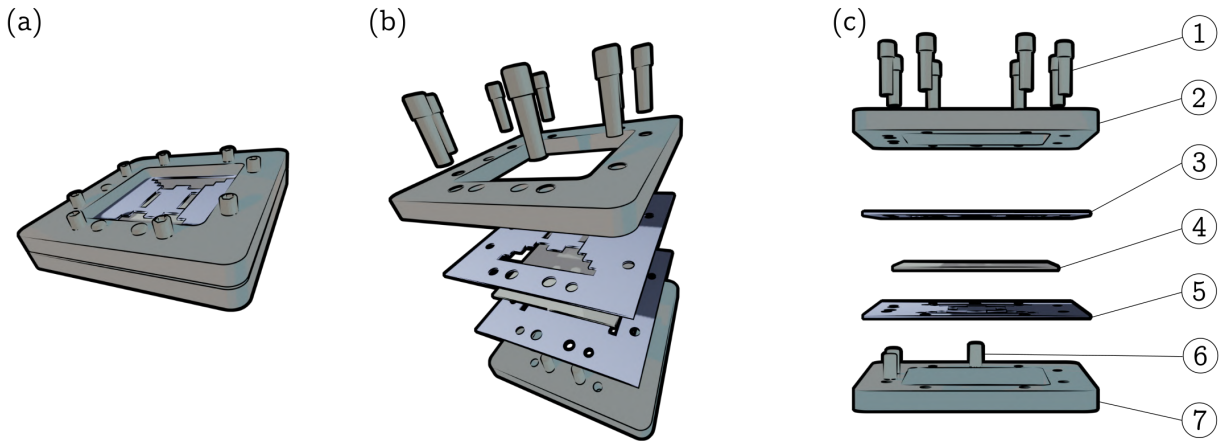

Figure 6.3 During treatment, the sample is placed in a steel jig: (a) A representation of the assembled jig; (b) a perspective representation of the disassembled jig; (c) a detailed representation of the disassembled jig. The cap screws (1) apply the clamping pressure to keep the sample from deforming during the treatment. The jig structure is comprised of a pair of steel frames (2 & 7). The jig further serves the purpose of holding and providing accurate registration of the laser cut cardstock masks that impose the peening pattern (3 & 5), as well as the registration of the sample (4), with the use of three steel dowel pins (6).

A prototype 2-axis shot peen forming robot (Figure 6.4) peens the fixed and masked plate, following a zig-zag path as depicted in Figure 6.2c. To ensure that the totality of the pattern is executed with the same process parameters the path needs to be executed at a constant speed. For this reason, the path of the robot is programmed to allow for acceleration and deceleration sequences to happen outside of the sample surface. To reduce the variance of the intensity parameters, only a single intensity is used during the scope of this work. Using multiple intensities would result in the modification of the air pressure (or the shot media) between iterations, introducing uncertainty, requiring additional calibration steps, and increasing the overall technical complexity. For this reason, only areas with an expansion value $\chi_i = 1$, as planned by the optimization algorithm, are treated. The programmed path executes a full pass over the surface of the sample. To increase the exposure time of the

sample to the impacts, multiple passes are required. Since this work focuses on iterative and repeatable treatment, the achievement of a full coverage is required. The term coverage refers to the percentage of the treated area that has been impacted (Kirk, 2007). At full coverage, the effect of the random fluctuations of the shot stream are negligible since impacts overlap on the surface of the sample.

The remaining factors to determine are the layer expansion magnitude and the number of required passes to reach the desired treatment. Since the shot peen forming process is based on repeated surface impacts, it leads to the work-hardening of the surface (Kirk, 2007). The longer the surface of a sample is treated at a given impact energy, the more its deformation rate will decrease. After a certain number of peening passes, the change in the shape of the plate will plateau, which is known as saturation. The shot peening industry uses the Almen test to determine the saturation intensity of a given treatment (SAE International, 2013). This test requires to incrementally peen standardized strips of SAE 1070 steel (Almen strips) and measure their deflection. Saturation is reached when the deflection converges within 10% of the previous measurement, when the exposure time doubles (SAE International, 2013; Kirk, 2007). The calibrated number of passes (or exposure time) is then used to form the actual workpiece of interest. In this work, we are interested in the effectiveness of the treatment on the sample, i.e. the magnitude of the expansion introduced in the sample by the treatment. We propose to calibrate the expansion magnitude experimentally on a sample plate identical to the plate of interest. The effectiveness of the chosen treatment is determined by uniformly peening a sample with increasing number of passes and measuring its deformation until the rate plateaus. The resulting deformed plate is measured. The expansion value is then computed by solving the optimization problem detailed in Section 6.2.6, with the measurements of the peened calibration sample as target. This strategy poses the expansion of the top layer, induced by the peening treatment, as a latent expansion. The number of passes required to reach the deformation rate plateau is then verified for each peen-

ing iterations of the samples by incrementally measuring the totality of the sample. This has the advantage of taking into account the shot stream fluctuations, that would otherwise harm the repeatability of the process. This proposed calibration sequence validates convergence of the effectiveness of the treatment of each peening pattern. To be measured, the plate needs to be removed from the clamping jig, to freely deform. The registration function of the jig is therefore necessary to ensure that the plate is repositioned accurately between measurements.

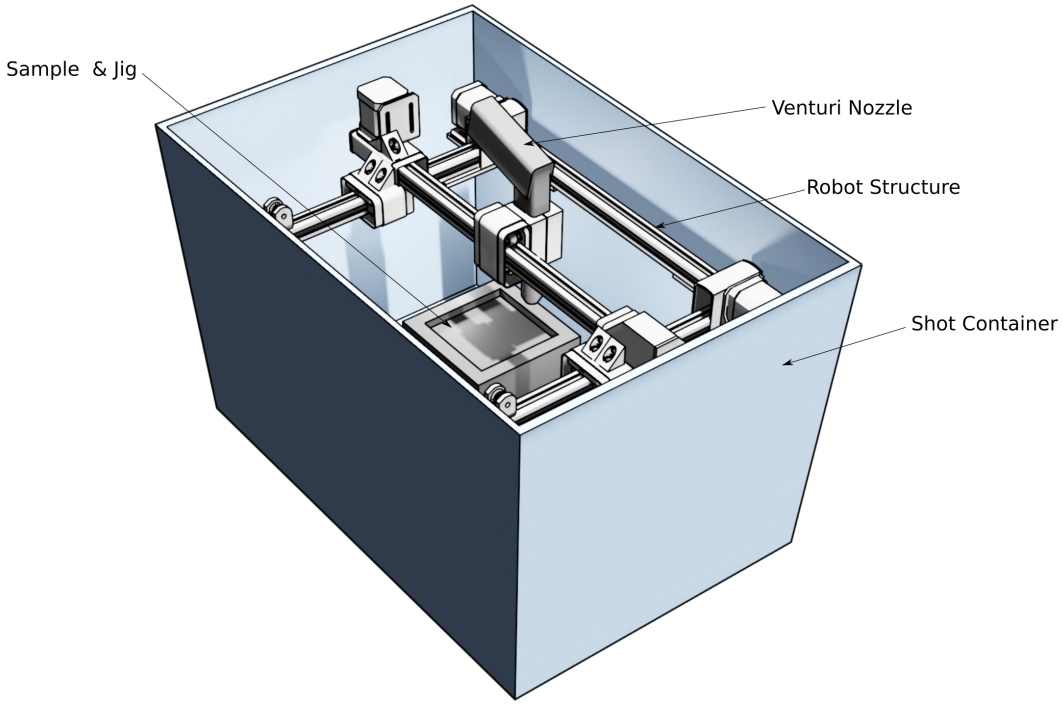

Figure 6.4 A rendered illustration of the prototype small scale shot peen forming robot: The setup consists of a structure of linear rails on which gantries move, controlled by stepper motors. The shot are propelled by a venturi nozzle (sandblasting nozzle). The gantries provide a range of motion of 150 mm in the x-axis and 110 mm in the y-axis. A plastic storage box contains the shot.

6.2.5 In-process measurement

The deformed plate is measured with a 0.001 mm resolution digital indicator mounted on a 3D printer, which acts as a low-cost measurement system as presented in Figure 6.5. The plate is placed on a holding jig which registers the sample with respect to the x- and y-axes of the printer and supports it from beneath, as illustrated in Figure 6.5a. This jig is comprised of a 3D printed structure with aluminum registration cylinders located at the corners, and four screws that serve as adjustable supports to conform to the samples shape. The 3D printer axes control the position of the indicator in the x-y plane, while the indicator measures the coordinate of a given point in the z-axis. The measurement grid matches the position of the nodes of the FEM mesh, to provide point-to-point correspondence between the measurements and the simulations. In the case of this work, since the FEM mesh consists of a grid of 16×16 structured square elements, the measurement sequence requires a grid of 17×17 equidistant points.

The repeatability of the measurement system is estimated by measuring the same sample 5 times, removing the sample from the holding jig, and putting it back, between measurements. The root mean square (RMS) of 5 calculated standard deviations for 289 measurement points (17×17) provides an estimate of the repeatability of the measurement method (ISO Central Secretary, 2008), bounding the standard statistical uncertainty of the set of 5 measurements to 0.027 mm. Throughout the process, the measurements are repeated 5 times and averaged, to respect the bounded uncertainty and to reduce the effect of random noise (Wang et al., 2015). The work origin is set as presented in Figure 6.5b, using the registration cylinders as reference. The work origin is kept constant for all measurements of the closed-loop, to remove this factor from the measurement uncertainty.

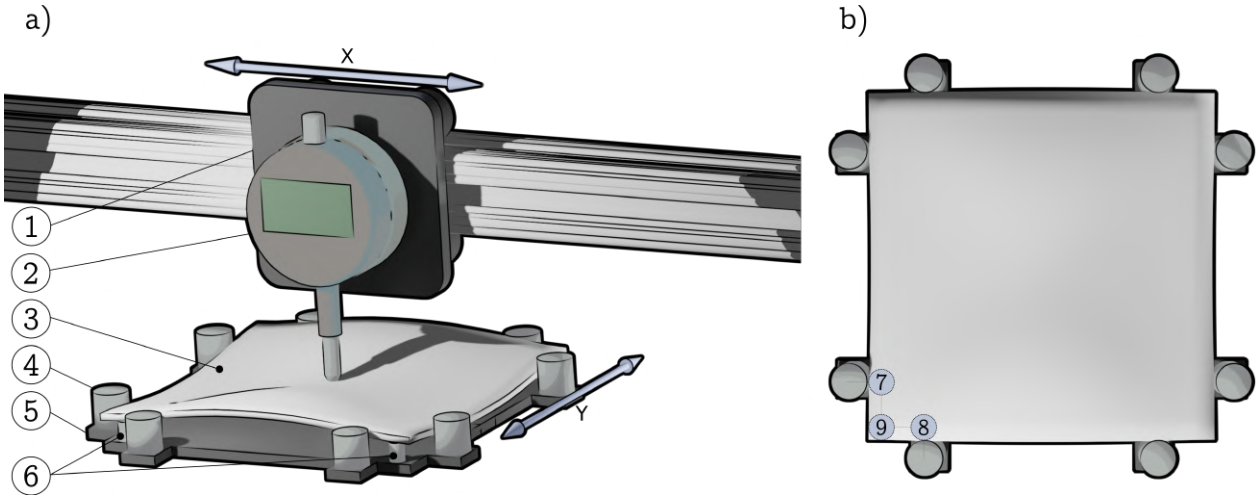

Figure 6.5 The measurement system: (a) The 3D printer gantry (1) holds the digital indicator (2) and controls its position on the global X axis. The sample (3) registered with respect to the system's X and Y axes with aluminum cylinders (4) mounted to a 3D printed jig (5). The sample is vertically supported by four screws (6), which provide a fine adjustment to adapt to the shape of the sample. The jig is mounted on the 3D printer bed, controlling the samples position on the system's y-axis; (b) The workpiece origin is defined in the lower left corner of the sample. The registration cylinders are used as reference. The x-axis origin is defined by the contact of the probe and the cylinder in (7) and the y-axis origin is defined by the contact of the probe and the cylinder in (8). The z-axis origin is defined in (9) when the probe engages with the surface of the sample. This workpiece origin is maintained for all measurement sequences of the same sample to remove this factor from the measurement uncertainty.

To be compared with the simulation results, the measured point cloud needs to be aligned with the simulation frame of reference, which corresponds to the global $[x, y, z]$ coordinate system. Since the holding jig physically registered the sample with respect to the x- and y-axes of the measurement system, only the z-axis coordinates are required to be numerically registered. The proposed method leverages a principal component analysis (PCA) (Chung et al., 1998) to compute the principal axes of the measured point cloud, i.e. the local coordinate system, and performs a system transformation of the z coordinates of the point cloud, setting the local $\bar{z}$-axis of the measurements, parallel to the global z-axis of the simulations. The PCA approach offers a simple solution to the registration problem with respect to the global coordinate system, which is readily available in the python library sckit-learn (Pedregosa et al., 2011). On the other hand, the PCA method is prone to flipping the principal

axis and by extension the data. To compensate for this problem an additional measurement point is added in one corner of the plate to serve as a landmark. This virtual landmark enables the user to verify if the point cloud is correctly oriented. If the point cloud is flipped, a simple 180deg rotation solves the issue. A rigid body translation then aligns the measurement center point to the simulation center node.

6.2.6 Replanning optimization

The measurements highlight the discrepancies with the shape expected by the bilayer model. Since the measures discussed in Section 6.2.4 are taken to ensure the repeatability of the shot peen forming process, we consider that the observed discrepancies are not likely to come from experimental sources. Rather, the presence of initial residual stresses provides a more compelling source of error. The following step of the proposed method is to explain the observed deviations, in terms of unknown expansions present in the bilayer plate. A modification to the optimization problem of Eq. 6.1 is proposed to estimate these error-inducing expansions. Its objective is to find the latent expansions (χ_{latent}) that minimize the vertical distance between the bilayer model and the measurements.

This optimization problem considers as starting point, the predicted shape of the bilayer from the first optimization problem. Then finds the equilibrium expansions that, combined with the applied expansions, explain the observed shape of the plate. In other terms, this process finds the expansions responsible for the forming error. The modified formulation of the optimization problem can be formulated as:

$$\begin{aligned} \underset{\chi \in R^n}{\text{minimize}} \, & \|z(\mathbf{x}, \mathbf{y}, \chi) - z_{measurement}(\mathbf{x}, \mathbf{y})\|_2^2 \\ \text{subject to} \quad & \chi_{\text{treated}} = 1 \\ & 0 \leq \chi_{\text{untreated}} \leq 1 \\ & \mathbf{A}^\top \chi \leq A_{max} \end{aligned} \tag{6.2}$$

where $z_{measurement}(\mathbf{x}, \mathbf{y})$ corresponds to the vertical coordinates of the measurements. χ_{treated} corresponds to the elements of the optimization vector χ which were peened so far. The constraint $\chi_{\text{treated}} = 1$ forces the elements that were treated to stay peened in the new optimization problem (shot peen forming cannot be undone). The constraint $0 \leq \chi_{\text{untreated}} \leq 1$ defines that all previously untreated elements can now have an expansion between 0 and 1, to be freely adjusted by the optimization algorithm. The constraint $\mathbf{A}^\top \chi \leq A_{max}$ is kept from the previous optimization problem to enforce realistic peening patterns.

The loop is reset by the computation of a new peening pattern to correct the observed error. The hypothesis behind the proposed method is that the observed shape of a plate is the result of the equilibrium of the expansions contained in the material. For this reason, the superposition of the expansions induced by the peen forming treatment and the latent expansions responsible for the observed discrepancies, define the observed shape of the plate. A corrective pattern can be computed by updating the bounds of the first optimization problem (Eq. 6.1) so that it writes:

$$\begin{aligned} \underset{\chi \in R^n}{\text{minimize}} \, & \|z(\mathbf{x}, \mathbf{y}, \chi) - z_{target}(\mathbf{x}, \mathbf{y})\|_2^2 \\ \text{subject to} \quad & \chi_{\text{treated}} = 1 \\ & \chi_{\text{latent}} \leq \chi_{\text{untreated}} \leq 1 \\ & \mathbf{A}^\top \chi \leq A_{max} \end{aligned} \tag{6.3}$$

The constraint $\chi_{\text{treated}} = 1$ forces the elements that were treated to stay peened. The term

χ_{latent} represents the unknown expansions estimated by optimization problem in Eq. 6.2. The constraint $\chi_{\text{latent}} \leq \chi_{\text{untreated}} \leq 1$ defines that all previously untreated elements can exhibit an expansion between χ_{latent} and 1, to be adjusted by the optimization algorithm.

The sample is further treated with the computed corrective pattern following the same procedure presented in Section 6.2.3. At each iteration, the elements of the corrective pattern are added to the vector χ_{treated}. The process is repeated until the optimization algorithm stops finding corrective patterns to reduce the forming error. This means that the optimization algorithm no longer finds a suitable pattern with the prescribed intensity. Beyond that point, considering a different treatment may have provided finer adjustments, but this is beyond the scope considered in this work.

6.3 Implementation results and discussion

6.3.1 Experimental test case

The performance of the proposed closed-loop method is demonstrated in an experimental test case in which the target is a saddle shape of 0.3 mm deflection. The saddle is a commonly used shape in peen forming studies (Faucheux, 2019; Luo et al., 2020; Miao et al., 2021) making it easier to compare with previously published work.

The present test case involves 6061-T6 plates of 1.04 mm (0.041") thickness, water jet cut to 76.2 $mm \times 76.2$ mm (3"×3"). The use of numerically controlled water jet cut process minimizes the variance between samples in residual stress induced by the cutting process. The test case results are presented for 3 samples, to demonstrate the robustness of the method to the initial stress state of the plates. The test case was conducted on an in-house shot peen forming robot. The robot projects the Zirshot Z425 ceramic shot with a venturi noz-

zle driven with compressed air at 75 psi. The robot is programmed to follow the zig-zag trajectory described in Section 4.2 and illustrated in Figure 6.2c, moving over the sample at a constant speed of 5 mm/s. Gariépy et al. (2013) demonstrated that the orientation of the peening path with respect to the lamination direction of the aluminum plate has an impact on the resulting curvature. Therefore, all samples in the test case are treated with a nozzle path that follows the lamination direction of the plate. The pattern is enforced during the treatment with a mask laser cut in a sheet of card stock. The closed-loop procedure is followed until the re-planning step proposes no further corrective patterns. This stopping criterion as opposed to stopping at a user-defined tolerance value allows to see the full extent of the proposed method's ability to reduce forming error.

6.3.2 Results

The Hausdorff distance (Taha and Hanbury, 2015) computed between the target shape nodes and the measurement points serves as error metric in this study. Figure 6.6 illustrates the 4 iterations that were required to reduce the Hausdorff distance of the first sample with respect to the target shape from 0.667 mm to 0.198 mm. Figure 6.6a and b present the patterns computed by the method for each iteration on the top and bottom face, respectively. In this representation, the blue regions correspond to the elements of the FEM that the optimization algorithm prescribed to be treated. Figure 6.6c and d present the overlaid cross-sections of the measurements and the target. This representation facilitates the visualization of the results and illustrates the progress of the deformed shape of the sample. Figure 6.6e presents the Hausdorff distance between the target shape and the measured shape. Overall, the Hausdorff distance decreases upon more iterations. From Iteration 2 to Iteration 3, a small increase in error is observed, which is then corrected in Iteration 4. We consider that this is explained by the algorithm exiting the local minimum of Iteration 2, allowing to reach a better solution once more information on the latent expansions was gathered. Based on the measurements of

Iteration 4, the optimization algorithm computed blank patterns for the top and the bottom faces of the plate, meaning that no further treatment would reduce the forming error.

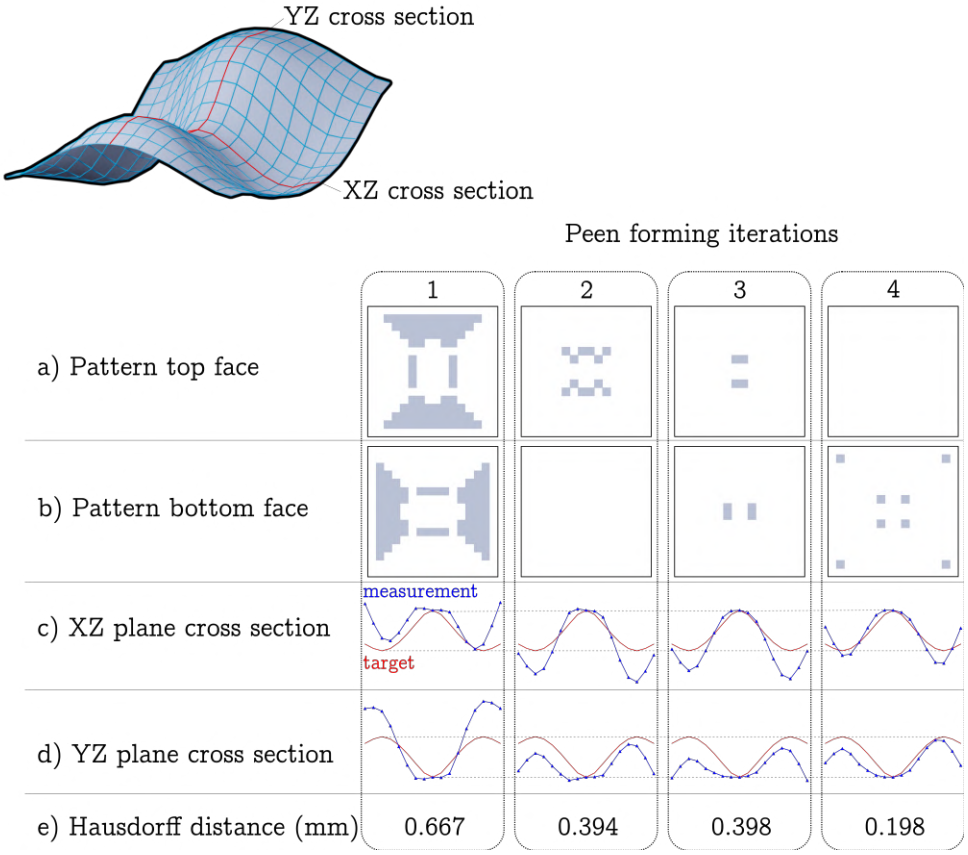

Figure 6.6 The performance of the closed-loop on sample 1 of the test case: a) the peening patterns predicted by the algorithm for the top face of the plate, the blue regions require treatment; b) the peening patterns predicted for the bottom face of the plate; c) the measurements of the plate along the XZ plane cross-section, referenced to the target shape cross-section; d) the measurements of the plate along the YZ plane cross-section, referenced to the target shape cross-section; e) the Hausdorff distances decreasing from 0.667 mm to 0.198 mm.

Figure 6.7 presents the results of the test case for the second sample. This sample required 3 iterations to bring the Hausdorff distance from 0.333 mm to 0.197 mm. This sample also exhibits a slight increase in error between Iterations 1 and 2 followed by a larger decrease in error with the third iteration. From the measurements for Iteration 3, the algorithm also provided no further peening pattern to be treated with the working intensity.

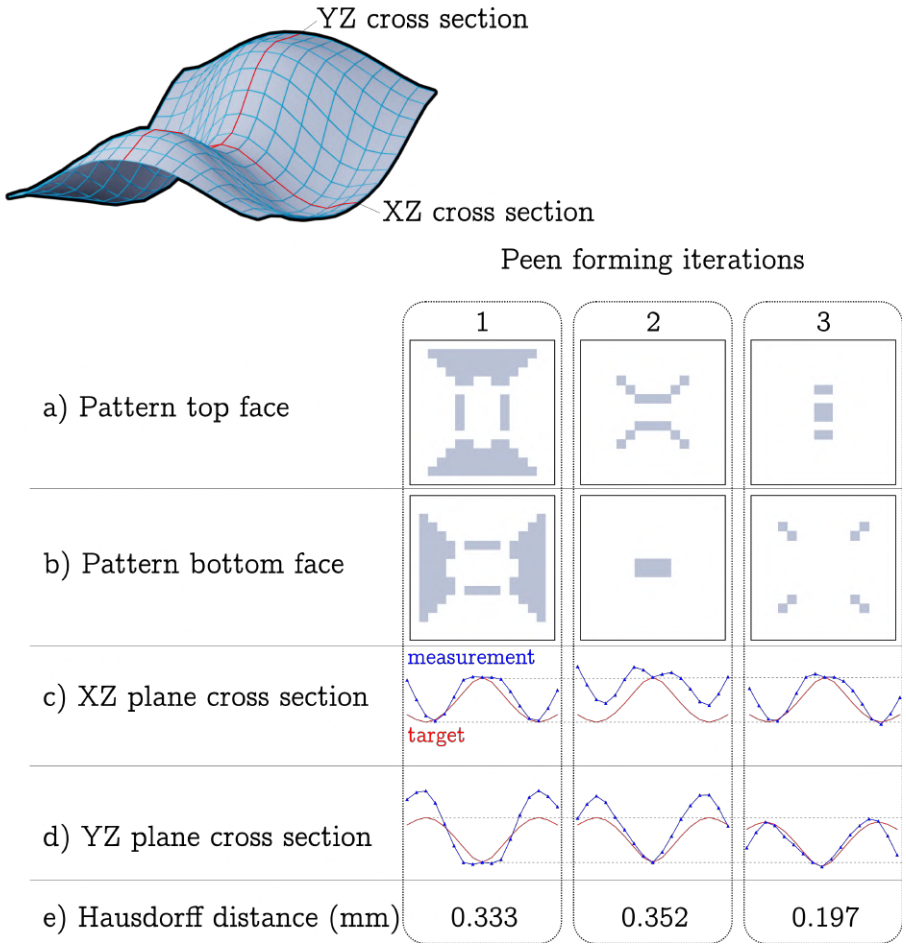

Figure 6.7 Results of the second sample of the test case: a) the peening patterns predicted by the algorithm for the top face of the plate; b) the peening patterns predicted for the bottom face of the plate; c) the measurements of the plate along the XZ plane cross-section, referenced to the target shape cross-section; d) the measurements of the plate along the YZ plane cross-section, referenced to the target shape cross-section; e) the Hausdorff distances decreasing from 0.333 mm to 0.197 mm.

Figure 6.8 presents a summary of the progression of the experimental closed loop on the three sample plates in terms of the Hausdorff distance. The first iteration displays identical peening patterns for the three samples since this corresponds to the initial peening, before feedback. Though the same peening pattern is enforced with the same methodology and process parameters, each sample exhibits a different shape and a different level of error with respect to the target. This is explained by the initial state of the samples. This observation is further supported by the fact that all three samples required a different number of peen forming iterations for the algorithm to converge to a solution that cannot be improved according to the simulation. Despite these variations, all three samples ended the process with Hausdorff distances below 0.2 mm, which demonstrates that the method is suitable to compensate for the initial state of the plate.

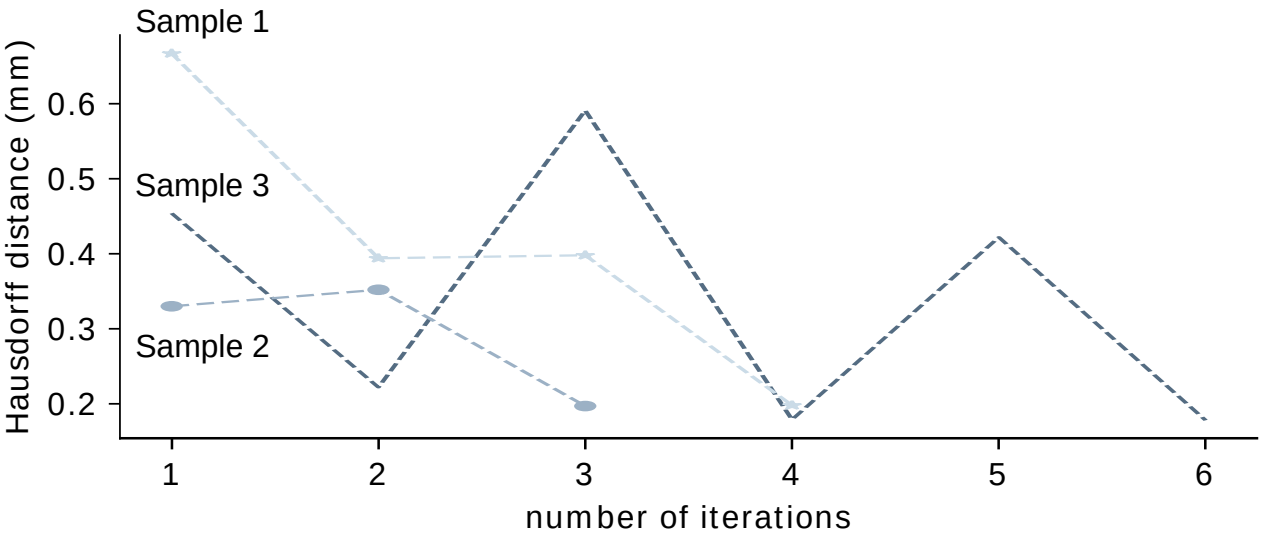

Figure 6.8 A summary of the progression of the closed-loop for the three samples. The graph presents the decrease of the Hausdorff distance between the measured plates and the target shape. Sample 1 required 4 peening iterations, sample 2 required 3 iterations and sample 3 required 6 iterations. All three samples exited the loop with errors below 0.2 mm.

6.3.3 Discussion

As shown by the summary presented in Figure 6.8, all three samples exhibit a varying degree of error oscillation, which can be explained by the exploratory nature of the closed-loop framework. At each iteration, a new plan is computed based on the information available through the iterative measurements of the sample and the memory of previously treated regions. In other terms, a decision is made at each step from incomplete information. The more the samples are treated, the more information on the global state of the material is gathered, which leads to the overall error reduction. The observed oscillations could be reduced by first performing the closed-loop at a lower process effectiveness aiming for a less deformed target. This initial step would act as a tentative inquiry of the effect of the initial state of the sample. With the lower effectiveness completed closed-loop sequence, a full effectiveness closed-loop sequence can be performed to reach the desired fully deformed target shape, with most of the oscillation causing latent expansions overridden by the lighter peening passes. While this may reduce the magnitude of the error oscillations, this idea raises the question of how much the effectiveness and target shape deflection need to be reduced.

Alternatively, the magnitude of oscillations could also be diminished by reducing the value of the overfit inhibiting constraint parameter A_{max} presented in Eq. 6.1 of Section 6.2.3. This strategy would force the optimization algorithm to plan for patterns covering less of the plate area at each iteration, therefore reducing the risk of over-peening the samples. This solution however may lead to requiring more iterations of the closed-loop to converge. From the results presented in the test case, the first planning iteration may have benefited from reducing the A_{max} value, since it yielded a peening pattern with a large area. However, the subsequent planning iterations all produced small patterns, meaning that the reduction of the total treated area may have a smaller effect. Moreover, an A_{max} value too small may cause the closed-loop to stop prematurely if no peening pattern small enough can be found to improve the current solution. Therefore, finding an efficient method to determine the A_{max}

value at each loop iteration may be required.

This work relied on two distance metrics: the node-to-node vertical distance between the FE mesh and the optimization target and the Hausdorff distance computed in euclidean space between the measurement points and the target shape nodes. The vertical distance was preferred within the mean squared error loss function of the planning steps, despite the predominant bending effect of shot peen forming. Intuitively, a curvature-based loss function may have been considered more efficient at capturing the main deformation mode of the process. However, a curvature-based loss function was rejected in this work due to the sensitivity issues introduced by such a higher-order quantity. Moreover, the use of a curvature-based loss function would not work with target shapes of constant curvature, since the gradient of the curvature would be zero at all points of the target shape. This would introduce a mean in the presence of a local minimum at the start of the optimization process, when the plate is flat.

Despite the fact that the planning and re-planning optimization steps of the closed-loop rely on a mean squared error-based loss function, the Hausdorff distance computed in euclidean space is preferred for the analysis of the test case because it represents the largest gap between the sample and the reference, which is more convenient to visualize and agrees with industry practices (Ramati et al., 1999). For the same practical reasons, the computation of the error metric in euclidean space, as opposed to curvature, is preferred, despite the predominant bending effect of shot peen forming.

The current study is limited to the case of simple square plates which are treated with a single peening intensity. The choice of a unique peening intensity was made to simplify the fabrication of the masks and limit the uncertainty regarding the repeatability of the process during the experimental test case. More intensities could have been considered in this work by producing intermediary masks and treating the plate with different pressures. The finite

element model harnessed throughout this work considers linear deformation behaviour, limiting the current implementation to small deformations. Since the induced deflections never exceeded 60 % of the sample thickness, the linear approximation is acceptable in the current situation. This work is also limited to symmetrical geometries and patterns due to the use of symmetry boundary conditions in the FEM. Removing these conditions would allow to further correct local errors that are not grasped by the symmetrical model.

6.4 Conclusion and outlook

This work demonstrates that the proposed closed-loop method consisting of a bilayer plate finite element model, combined with optimization and in-process measurements significantly reduces shot peen forming errors, when compared with the standard feedback-less forming method. The proposed method is founded on the hypothesis that the shape of a peen-formed plate is the result of an equilibrium of expansion-induced bending moments. We leverage this hypothesis to introduce the notion of latent expansions that are used to explain observed discrepancies between the simulations and the measurements. The latent expansions serve in further planning steps to compute corrective patterns.

The concept of latent expansions introduced in this work served as fictitious expansions computed by optimization to convey the measured errors to the planning algorithm. They were not presented as approximations of the initial residual stresses present in the material. Despite this fact, the investigation of the correlation between latent expansions and initial residual stresses presents an interesting avenue for future work.

In an industrial application of shot peen forming, this method could be harnessed to reduce forming errors until a part respects the specified tolerance and serve as the foundation for a fully automated peen forming process. The proposed method could further be adapted to

consider more complex machined parts and therefore provide more insights for current industrial challenges. For instance, the extension of this work to integrally stiffened aluminum panels could still rely on the bilayer plate model to simulate both the main panel and the thin stiffeners. Both planning and re-planning steps could maintain their use of the interior points algorithm and the notion of latent expansions. However, such more complex geometry would require alterations to the experimental setup methodology, such as finding an alternative to the card stock masks, using more complex holding fixtures and using a robotic system with more than two degrees of freedom.

Acknowledgements

This work was funded by Aerosphere Inc., the Fonds de recherche du Québec – Nature et technologies and the ministère de l'Économie, de la Science et de l'Innovation [Funding reference number LU-210888]. The authors would like to thank Dr. Hong-Yan Miao for her insightful comments that improved the manuscript.

CHAPTER 7 GENERAL DISCUSSION

7.1 Summary of findings

The literature review in Chapter 2 presented that there are currently available methods to simulate and plan the shot peen forming process. The planning methods described rely on the iterative use of simulation methods to compute the required peening pattern and effectiveness to reach a target shape. Chapter 4 presented a planning method based on an artificial neural network trained on finite element simulations. With the proposed workflow, the computationally expensive iterations are executed offline, making the in-process planning happen in real-time. This contribution displayed a proof of concept on square plates with symmetrical target shapes that require complex peening patterns to reach. This study was limited to single-sided peening.

The second contribution presented in Chapter 5 of this manuscript was motivated by the high barrier to entry in the field of shot peen forming research. The literature review highlighted that the automated shot peen forming industry and research community rely on industrial robots housed in large basting cabinets. Though it is logical for handling large parts and high volumes, this approach is not necessary for researchers working on small samples to experimentally validate their methods. The proposed shot peen forming robot has for objective to lower the costs for researchers to get experimental results and iterate faster than would be possible with a standard robot and blasting cabinet acquisition process. It also provides an easily customizable platform to test new auxiliary equipment.

The literature review further highlighted that the presence of initial residual stresses in parts is the main source of shot peen forming error. The currently available planning and simulation methods do not account for this initial stress state. Since the measurement of residual stresses is either expensive or destructive, Chapter 6 proposed a closed-loop scheme that iteratively compensates for the initial measured shape error, using in-process shape measurements and optimization. From

these measurements, the closed-loop computes what we coined latent expansions, which represent the missing expansions that balance the effects of the shot peening treatment to explain the measured error. These latent expansions are computed using a modified planning optimization problem. The concept of latent expansions is based on the postulates that all peen-formed shapes are the result of an equilibrium of bending moments. From the latent expansions, a new peening plan is computed to negate their effect on the plate. The new plan is executed and the loop is continued until no improvement is possible. This method was validated in an experimental test case presented in Chapter 6. This test case demonstrated that the proposed method was able to reduce the initial forming error of three 3" $\times$ 3" $\times$ 0.041" 6061-T6 plates below 0.2 mm. It also demonstrated that even though the same initial pattern was used for all samples, they exhibited different initial errors, which hints at a variation in initial state. This study was also limited to square plates, although the method is readily extendable to more geometries. This study also leveraged symmetries to reduce the computation cost of the simulations. Evidently, a choice was made to deviate from the use of neural networks to plan shot peen forming, and focus on an optimization-based planning method in Chapter 6. However, using a neural network as part of a closed-loop scheme for shot peen forming automation could be explored in the future, as explained in Section 7.2.

7.2 Recommendation for future work

Recommendations for extensions to the presented work can be separated into incremental improvements and paradigm-shifting improvements. Incremental improvements focus on the immediate limitations presented in the previous section. Notably removing the use of symmetries in all the proposed methods. The symmetry hypothesis was considered to facilitate the development and validation of the solutions. With the methods validated, one could implement the same methods without the symmetries and improve them without changing the core concepts.

The presented contributions all involved small plates. Extending the proposed methods to larger square plates involves greater implementation challenges in the design and fabrication of fixtures,

but does not involve important scientific barriers. Extending the proposed methods to more complex geometries such as integrally stiffened panels would bring the closed-loop scheme and planning methods closer to current industrial needs. Such an extension would require more work than scaling the size of the panel, but would maintain the core idea of the proposed methods. The main challenge with such extension would be in the experimental phase of the work. Notably the manufacturing of the parts, the design of proper work holding able to maintain the part flat during the treatment, and mostly the development of a method for repeatably imposing the correct peening pattern on complex parts. Furthermore, to extend this work to complex geometries, one could not rely on the 2-axis shot peening robot presented in Chapter 5, with the addition of features in the third dimension. The proposed robot would either require modifications to accommodate more complex geometries, or the use of an industrial robot would be required.

The use of laser-cut cardstock masks allowed to precisely impose the required peening pattern on sample plates, with good correspondence between the simulation and the imposed pattern. This was an efficient solution due to the small scale of the samples and an improvement over the existing methods using hand-cut tape, but for large industrial parts, this method may not scale. The use of a flap system as presented in section 2.7 of the literature review would be more suitable for large components. However, the use of masks has the advantage of decoupling the pattern resolution and the nozzle size, which can be a limiting factor for small parts, or high-resolution patterns. It also enables the decoupling of the robot path and the peening pattern, removing the need to replan the robot path for each forming iteration.

The neural network planning method proposed in Chapter 4 presents an opportunity for future work that would require a shift in automation paradigm. The advantage of using a neural network as a planner is its ability to be updated when trained with new data. The field of Deep Reinforcement Learning leverages this feature to develop models that are updated by interacting with a given task. This concept was demonstrated in robotic manipulation applications (Nguyen and La, 2019) in which a neural network was trained by interacting with a robot (real or simulated) to control its joint motions to perform a determined manipulation task. In this context, the neural network

had to approximate the mechanics that govern the robot's motion through trial and error. Tobin et al. (2017) further proposed to train the neural network in simulation with randomized physical parameters such as the mass of the robot and the friction coefficients of the involved surfaces, to derive a model robust to unknown physical parameters. Given this, it could be possible to extend the neural network proposed in this work to be robust to unknown initial stresses by training it in a virtual environment with randomized initial states using the concepts of deep reinforcement learning. This scheme would support the analogy to the human operator learning to compensate for variations from unknown parameters through trial and error. The main limitation of these data-based methods is the requirement for a large quantity of data. In the case of applying them to shot peen forming, that would imply performing large quantities of experiments, or relying on simulations alone.

CHAPTER 8 CONCLUSION

This thesis took a critical look at the current state of shot peen forming in the aerospace manufacturing industry. It is at the time still a highly manual process relying on human intuition. This is opposed by the industrial need for higher repeatability and accuracy. While automation has the potential to fill these needs, the information on the topic of shot peen forming automation is mostly hidden behind industrial secrecy due to its competitive advantage. Academic research on the other hand strives to openly disseminate knowledge for others to build upon it and further the collective expertise. Academic research on the topic of shot peen forming has mostly focused on the development of tools to simulate and plan the process, but little has been done on the topic of fully automated shot peen forming. The goal of this manuscript was to offer a suitable solution to the problem of closed-loop automation of shot peen forming in the hope that it will further stimulate the development of automated shot peen forming to answer industrial needs.

Solving non-linear problems in real-time has been simplified with advances in machine learning. In this thesis, we also demonstrated that this burgeoning technology can be applied to the planning of shot peen forming in predicting required shot peening patterns to reach the desires shape. This contribution lays the groundwork for more advanced real-time planning solutions based on artificial neural networks. It can be noted that the adjacent field of Deep Reinforcement Learning offers the potential to further improve the real-time planning of shot peen forming by learning the non-linear functions that dictate the process by interacting with it.

The manuscript further highlighted the technical obstacles that hinder the implementation of fully automated shot peen forming, such as the effect of initial residual stresses in parts. We proposed the solution of a closed-loop approach to compensate for the error introduced by initial stresses through replanning based on in-process shape measurements. This solution was deemed suitable through experimental validation, but the presented implementation remains limited to plates. It is possible to imagine the extension of this method to more complex parts to consider it viable for

real-life industrial settings.

The rapid adoption of 3D printers in domestic settings has increased the development rate of the process. This adoption was possible due to the decreasing of the barrier to entry in the field in terms of accessibility to the hardware. As a side effect, 3D printing research is now more affordable. In the context of shot peen forming, the same observation is not possible. The equipment to automate shot peen forming remains expensive. This manuscript presents a low-cost open-source shot peen forming system suitable to perform experimental validation on small samples. The objective of this contribution is to lower the entry costs for researchers wanting to contribute to the shot peen forming research. This design was distributed as an open-source project in the hope of increasing the number of openly available contributions in the field of shot peen forming automation.

REFERENCES

Martín Abadi, Ashish Agarwal, Paul Barham, Eugene Brevdo, Zhifeng Chen, Craig Citro, Greg S. Corrado, Andy Davis, Jeffrey Dean, Matthieu Devin, Sanjay Ghemawat, Ian Goodfellow, Andrew Harp, Geoffrey Irving, Michael Isard, Yangqing Jia, Rafal Jozefowicz, Lukasz Kaiser, Manjunath Kudlur, Josh Levenberg, Dandelion Mané, Rajat Monga, Sherry Moore, Derek Murray, Chris Olah, Mike Schuster, Jonathon Shlens, Benoit Steiner, Ilya Sutskever, Kunal Talwar, Paul Tucker, Vincent Vanhoucke, Vijay Vasudevan, Fernanda Viégas, Oriol Vinyals, Pete Warden, Martin Wattenberg, Martin Wicke, Yuan Yu, and Xiaoqiang Zheng. TensorFlow: Large-scale machine learning on heterogeneous systems, 2015. URL `https://www.tensorflow.org/`. Software available from tensorflow.org.

Silas Alben, Bavani Balakrisnan, and Elisabeth Smela. Edge effects determine the direction of bilayer bending. *Nano letters*, 11(6):2280–2285, 2011.

Byoungkwon An, Ye Tao, Jianzhe Gu, Tingyu Cheng, Xiang Anthony Chen, Xiaoxiao Zhang, Wei Zhao, Youngwook Do, Shigeo Takahashi, Hsiang-Yun Wu, Teng Zhang, and Lining Yao. Thermorph: Democratizing 4d printing of self-folding materials and interfaces. In *Proceedings of the 2018 CHI Conference on Human Factors in Computing Systems*, CHI '18, pages 1–12, New York, NY, USA, 2018. Association for Computing Machinery. ISBN 9781450356206. doi: 10.1145/3173574.3173834. URL `https://doi.org/10.1145/3173574.3173834`.

Basile Audoly and Yves Pomeau. *Elasticity and geometry: from hair curls to the non-linear response of shells*. Oxford university press, 2010.

Patrick Ballard. *Contraintes résiduelles induites par impact rapide. Application au choc-laser*. PhD thesis, Ecole Polytechnique X, 1991.

Bill Barker. Shot peening small holes. *Shot Peener(USA)*, 15(4):4–8, 2001.

J. L. Batoz and G. Dhatt. Development of two simple shell elements. *AIAA Journal*, 10:237–238, 1972.

Rémi Bonin, Farbod Khameneifar, and JRR Mayer. Evaluation of the metrological performance of a handheld 3d laser scanner using a pseudo-3d ball-lattice artifact. *Sensors*, 21(6):2137, 2021.

Stephen Boyd, Stephen P Boyd, and Lieven Vandenberghe. *Convex optimization*. Cambridge university press, 2004.

Richard H. Byrd, Mary E. Hribar, and Jorge Nocedal. An interior point algorithm for large-scale nonlinear programming. *SIAM Journal on Optimization*, 9(4):877–900, 1999. doi: 10.1137/S1052623497325107. URL `https://doi.org/10.1137/S1052623497325107`.

W Cao, R Fathallah, and L Castex. Correlation of almen arc height with residual stresses in shot peening process. *Materials science and Technology*, 11(9):967–973, 1995.

Thibaut Chaise, Jun Li, Daniel Nélias, Régis Kubler, Said Taheri, Gérard Douchet, Vincent Robin, and Philippe Gilles. Modelling of multiple impacts for the prediction of distortions and residual stresses induced by ultrasonic shot peening (usp). *Journal of Materials Processing Technology*, 212 (10):2080–2090, 2012.

Jack Champaigne. Shot peening process variables. *Shot Peener*, 7(3):16, 1993.

Zhuo Chen, Fan Yang, and SA Meguid. Realistic finite element simulations of arc-height development in shot-peened almen strips. *Journal of Engineering Materials and Technology*, 136(4), 2014.

François Chollet et al. Keras. `https://keras.io`, 2015.

Do Hyun Chung, Il Dong Yun, and Sang Uk Lee. Registration of multiple-range views using the reverse-calibration technique. *Pattern Recognition*, 31(4):457–464, 1998. ISSN 0031-3203. doi: https://doi.org/10.1016/S0031-3203(97)00063-0. URL `https://www.sciencedirect.com/science/article/pii/S0031320397000630`.

Thomas H. Cormen, Charles E. Leiserson, Ronald L. Rivest, and Clifford Stein. *Introduction to Algorithms, Third Edition*. The MIT Press, 3rd edition, 2009. ISBN 0262033844.

Sergio Delijaicov, AT Fleury, and FPR Martins. Application of multiple regression and neural networks to synthesize a model for peen forming process planning. *Journal of Achievements in Materials and Manufacturing Engineering*, 43(2):651–656, 2010.

Guido Dhondt. *The Finite Element Method for Three-Dimensional Thermomechanical Applications*. John Wiley & Sons, November 2004. ISBN 978-0-470-85762-5.

Pierre Faucheux. Simulating shot peen forming with eigenstrains (phd thesis), 2019. URL `https://publications.polymtl.ca/4189/`.

Pierre A. Faucheux, Frédérick P. Gosselin, and Martin Lévesque. Simulating shot peen forming with eigenstrains. *Journal of Materials Processing Technology*, 254:135 – 144, 2018. ISSN 0924-0136. doi: https://doi.org/10.1016/j.jmatprotec.2017.11.036. URL `http://www.sciencedirect.com/science/article/pii/S0924013617305563`.

Axel Friese. Ksa develops new automated peen forming for wing skins. *Shot Peener*, 14(6088): 16–17, 2006. ISSN 1476-4687. URL `https://www.shotpeener.com/library/pdf/2006031.pdf`.

Axel Friese, Jürgen Lohmar, and Frank Wustefeld. Current applications of advanced peen forming implementation. *Shot Peening*, 2002:53–57, 2002.

A Gariépy, S Larose, C Perron, P Bocher, and M Lévesque. On the effect of the orientation of sheet rolling direction in shot peen forming. *Journal of Materials Processing Technology*, 213(6): 926–938, 2013a.

A Gariépy, S Larose, C Perron, P Bocher, and M Lévesque. On the effect of the peening trajectory in shot peen forming. *Finite Elements in Analysis and Design*, 69:48–61, 2013b.

A. Gariépy, S. Larose, C. Perron, and M. Lévesque. Shot peening and peen forming finite element modelling – towards a quantitative method. *International Journal of Solids and Structures*, 48 (20):2859–2877, 2011. ISSN 0020-7683. doi: https://doi.org/10.1016/j.ijsolstr.2011.06.003. URL `https://www.sciencedirect.com/science/article/pii/S0020768311002137`.

A. Gariépy, S. Larose, C. Perron, P. Bocher, and M. Lévesque. On the effect of the orientation of sheet rolling direction in shot peen forming. *Journal of Materials Processing Technology*, 213

(6):926–938, 2013. ISSN 0924-0136. doi: https://doi.org/10.1016/j.jmatprotec.2013.01.003. URL https://www.sciencedirect.com/science/article/pii/S0924013613000113.

Pooya Ghandali, Farbod Khameneifar, and JRR Mayer. A pseudo-3d ball lattice artifact and method for evaluating the metrological performance of structured-light 3d scanners. *Optics and Lasers in Engineering*, 121:87–95, 2019.

Ian Goodfellow, Yoshua Bengio, and Aaron Courville. *Deep Learning*. MIT Press, 2016. http://www.deeplearningbook.org.

Alain Goriely. *The mathematics and mechanics of biological growth*, volume 45. Springer, 2017.

LV Grasty and C Andrew. Shot peen forming sheet metal: Finite element prediction of deformed shape. *Proceedings of the Institution of Mechanical Engineers, Part B: Journal of Engineering Manufacture*, 210(4):361–366, 1996. doi: 10.1243/PIME_PROC_1996_210_129_02. URL https://doi.org/10.1243/PIME_PROC_1996_210_129_02.

Edward Greig. Random maze generator, January 2016. URL https://github.com/Metallicow/Random_Maze_Generator.

Kalina T. Haas, Raymond Wightman, Elliot M. Meyerowitz, and Alexis Peaucelle. Pectin homogalacturonan nanofilament expansion drives morphogenesis in plant epidermal cells. *Science*, 367 (6481):1003–1007, February 2020.

Abdelfetah Hentout, Mustapha Aouache, Abderraouf Maoudj, and Isma Akli. Human–robot interaction in industrial collaborative robotics: a literature review of the decade 2008–2017. *Advanced Robotics*, 33(15-16):764–799, 2019.

SE Homer and RD Van Luchene. Aircraft wing skin contouring by shot peening. *Journal of materials shaping technology*, 9(2):89–101, 1991.

Sergey Ioffe and Christian Szegedy. Batch normalization: Accelerating deep network training by reducing internal covariate shift, 2015. URL http://arxiv.org/abs/1502.03167.

ISO Central Secretary. Uncertainty of measurement — part 3: Guide to the expression of uncertainty in measurement (gum:1995). Standard ISO/IEC GUIDE 98-3:2008, International Organization for Standardization, Geneva, CH, 2008. URL `https://www.iso.org/standard/50461.html`.

Hongzhi Jiang, Huijie Zhao, and Xudong Li. High dynamic range fringe acquisition: a novel 3-d scanning technique for high-reflective surfaces. *Optics and Lasers in Engineering*, 50(10): 1484–1493, 2012.

MT Khabou, L Castex, and G Inglebert. The effect of material behaviour law on the theoretical shot peening results. *European journal of mechanics. A. Solids*, 9(6):537–549, 1990.

Diederik P. Kingma and Jimmy Ba. Adam: A method for stochastic optimization, 2014. URL `http://arxiv.org/abs/1412.6980`.

David Kirk. Shot peening. *Aircraft engineering and aerospace technology*, 1999.

David Kirk. Peening intensity curves. *The Shot Peener*, 21(3):24–30, 2007. URL `https://www.shotpeener.com/library/pdf/2007020.pdf`.

Alex Krizhevsky, Ilya Sutskever, and Geoffrey E Hinton. *ImageNet Classification with Deep Convolutional Neural Networks*. Curran Associates, Inc., 2012.

Kishor M. Kulkarni, John A. Schey, and Douglas V. Badger. Investigation of shot peening as a forming process for aircraft wing skins. *Journal of Applied Metalworking*, 1(4):34–44, 1981.

Douglas Lanman and Gabriel Taubin. Build your own 3d scanner: 3d photography for beginners. In *ACM SIGGRAPH 2009 Courses*, pages 1–94. 2009.

Yann Lecun, Léon Bottou, Yoshua Bengio, and Patrick Haffner. Gradient-based learning applied to document recognition. In *Proceedings of the IEEE*, pages 2278–2324, 1998.

Andrew Levers and Alan Prior. Finite element analysis of shot peening. *Journal of Materials Processing Technology*, 80:304–308, 1998.

Yadong Li and Peihua Gu. Free-form surface inspection techniques state of the art review. *Computer-Aided Design*, 36(13):1395–1417, 2004.

Sacha Lifszyc. mazesolver, October 2013. URL `https://github.com/sachalifs/mazesolver`.

Shengjun Liu, Kwan-Chung Chan, and Charlie CL Wang. Iterative consolidation of unorganized point clouds. *IEEE computer graphics and applications*, 32(3):70–83, 2011.

Mingsheng Luo, Yongxiang Hu, Lan Hu, and Zhenqiang Yao. Efficient process planning of laser peen forming for complex shaping with distributed eigen-moment. *Journal of Materials Processing Technology*, 279:116588, 2020.

Marlin. Marlin firmware, 2021.

Hong Y Miao, Martin levesque, and Frederick Gosselin. Optimization of shot peen forming patterns to achieve complex target shapes the inverse problem, Apr 2021. URL `engrxiv.org/a2frz`.

HY Miao, S Larose, C Perron, and M Lévesque. On the potential applications of a 3d random finite element model for the simulation of shot peening. *Advances in Engineering software*, 40(10): 1023–1038, 2009.

MRX. X-raybot, 2021. URL `http://mrxrays.com/prototype1/`.

Hai Nguyen and Hung La. Review of deep reinforcement learning for robot manipulation. In *2019 Third IEEE International Conference on Robotic Computing (IRC)*, pages 590–595. IEEE, 2019.

Van Bo Nguyen, Augustine Teo, Te Ba, Ampara Aramcharoen, Kunal Ahluwalia, Si Bui Quang Tran, and Chang Wei Kang. Advanced model-based controller for cyber-physical shot peening process. *The International Journal of Advanced Manufacturing Technology*, pages 1–15, 2021.

Kazuyuki Oguri. Fatigue life enhancement of aluminum alloy for aircraft by fine particle shot peening (fpsp). *Journal of Materials Processing Technology*, 211(8):1395–1399, 2011.

David Palousek, Milan Omasta, Daniel Koutny, Josef Bednar, Tomas Koutecky, and Filip Dokoupil. Effect of matte coating on 3d optical measurement accuracy. *Optical Materials*, 40:1–9, 2015.

F. Pedregosa, G. Varoquaux, A. Gramfort, V. Michel, B. Thirion, O. Grisel, M. Blondel, P. Prettenhofer, R. Weiss, V. Dubourg, J. Vanderplas, A. Passos, D. Cournapeau, M. Brucher, M. Perrot,

and E. Duchesnay. Scikit-learn: Machine learning in Python. *Journal of Machine Learning Research*, 12:2825–2830, 2011.

Matteo Pezzulla, Gabriel P. Smith, Paola Nardinocchi, and Douglas P. Holmes. Geometry and mechanics of thin growing bilayers. *Soft Matter*, 12(19):4435–4442, 2016.

Flavio Prieto, Tanneguy Redarce, Richard Lepage, and Pierre Boulanger. An automated inspection system. *The International Journal of Advanced Manufacturing Technology*, 19(12):917–925, 2002.

Michael B Prime and Michael R Hill. Residual stress, stress relief, and inhomogeneity in aluminum plate. *Scripta Materialia*, 46(1):77–82, 2002.

C. Qi, Hao Su, Kaichun Mo, and L. Guibas. Pointnet: Deep learning on point sets for 3d classification and segmentation. *2017 IEEE Conference on Computer Vision and Pattern Recognition (CVPR)*, pages 77–85, 2017.

S Ramati, S Kennerknecht, and G Levasseur. Single piece wing skin utilization via advanced peen forming technologies, 1999. URL `http://www.aerosphere.ca/docs/ICSP-7.pdf`.

RepRap. Ramps 1.4 — reprap, 2021.

Joseph Ross, Kevin Harding, and Eric Hogarth. Challenges faced in applying 3d noncontact metrology to turbine engine blade inspection. In *Dimensional Optical Metrology and Inspection for Practical Applications*, volume 8133, page 81330H. International Society for Optics and Photonics, 2011.

David E. Rumelhart, Geoffrey E. Hinton, and Ronald J. Williams. Learning representations by back-propagating errors. *Nature*, 323(6088):533–536, 1986. ISSN 1476-4687. doi: 10.1038/323533a0. URL `https://www.nature.com/articles/323533a0`.

SAE International. Test strip, holder, and gage for shot peening. Standard, SAE International, 2013. URL `https://doi.org/10.4271/j442_201302`.

G. S. Schajer. *Practical Residual Stress Measurement Methods*. John Wiley & Sons, 2013.

Evan Shelhamer, Jonathan Long, and Trevor Darrell. Fully convolutional networks for semantic segmentation. *IEEE Transactions on Pattern Analysis and Machine Intelligence*, 39:640–651, 2017.

Wassime Siguerdidjane, Farbod Khameneifar, and Frédérick P Gosselin. Efficient planning of peen-forming patterns via artificial neural networks. *Manufacturing Letters*, 25:70–74, 2020.

Wassime Siguerdidjane, Farbod Khameneifar, and Frédérick P Gosselin. A low-cost open-source automated shot peen forming system. *HardwareX, (submitted for publication)*, 2021.

A. A. Taha and A. Hanbury. An efficient algorithm for calculating the exact hausdorff distance. *IEEE Transactions on Pattern Analysis and Machine Intelligence*, 37(11):2153–2163, 2015.

RJD Tatton. Shot peen-forming. *Elsevier Applied Science Publishers Ltd,*, pages 134–143, 1986.

Josh Tobin, Rachel Fong, Alex Ray, Jonas Schneider, Wojciech Zaremba, and Pieter Abbeel. Domain randomization for transferring deep neural networks from simulation to the real world. In *2017 IEEE/RSJ international conference on intelligent robots and systems (IROS)*, pages 23–30. IEEE, 2017.

T. Tommasi, N. Patricia, B. Caputo, and T. Tuytelaars. A deeper look at dataset bias. *ArXiv*, abs/1505.01257, 2015.

C. Van Der Malsburg. Frank rosenblatt: Principles of neurodynamics: Perceptrons and the theory of brain mechanisms. In Günther Palm and Ad Aertsen, editors, *Brain Theory*, pages 245–248, Berlin, Heidelberg, 1986. Springer Berlin Heidelberg. ISBN 978-3-642-70911-1.

Wim M. van Rees, Etienne Vouga, and L. Mahadevan. Growth patterns for shape-shifting elastic bilayers. *Proceedings of the National Academy of Sciences*, 114(44):11597–11602, 2017.

R. D. VanLuchene and E. J. Cramer. Numerical modeling of a wing skin peen forming process. *Journal of materials engineering and performance*, 5(6):753–760, 1996.

Jian Wang, Richard K. Leach, and X. Jiang. Review of the mathematical foundations of data fusion techniques in surface metrology. *Surface Topography: Metrology and Properties*, 3(2):023001, 2015. ISSN 2051-672X. doi: 10.1088/2051-672X/3/2/023001. Publisher: IOP Publishing.

Frank Wüstefeld, Wolfgang Linnemann, and Stefan Kittel. Towards peen forming process automation. *Shot Peening*, page 44, 2006.

Xudong Xiao, Yao Sun, Xin Tong, Yan Li, and Guoqiang Gao. Prediction of peen forming stress and plate deformation with a combined method. *Proceedings of the Institution of Mechanical Engineers, Part B: Journal of Engineering Manufacture*, 233(14):2492–2504, 2019a. ISSN 0954-4054, 2041-2975. doi: 10.1177/0954405419840549. URL `http://journals.sagepub.com/doi/10.1177/0954405419840549`.

Xudong Xiao, Xin Tong, Yao Sun, Yan Li, Shengmin Wei, and Guoqiang Gao. An analytical model for predicting peening stresses with general peening coverage. *Journal of Manufacturing Processes*, 45:242–254, 2019b. ISSN 1526-6125. doi: https://doi.org/10.1016/j.jmapro.2019.06.029. URL `https://www.sciencedirect.com/science/article/pii/S1526612518306108`.

Qingnan Zhou. Pymesh. `https://pymesh.readthedocs.io/en/latest/`, 2018.